UNIVERSITÀ DEGLI STUDI DI PADOVA

Dipartimento di Ingegneria Industriale DII

Corso di Laurea Magistrale in Ingegneria Aerospaziale

DESIGN OF A COUPLING SURFACE AS ALIGNMENT-AID FOR AN ANDROGYNOUS INTERFACE

Supervisor:

Univ.-Prof. Dr.-Ing. Mirco Zaccariotto
DII, Università degli Studi di Padova

External Supervisor(s):

Univ.-Prof. Dr.-Ing. Kai-Uwe Schröder
Dipl.-Ing. Thomas A. Schervan
SLA, RWTH Aachen

Author:

Marco Bissaro
1183103

Padova, September 2020

UNIVERSITÀ
DEGLI STUDI
DI PADOVA

Master Thesis

DESIGN OF A COUPLING SURFACE AS ALIGNMENT-AID OF AN ANDROGYNOUS ITERFACE

Declaration of autonomy

I hereby declare that I have written the following Master thesis myself. I declare that I have used no sources or aids but those stated, and that I have marked all the statements that have been taken from other works as such.

Padova, 13th October 2020 _____

(Signature)

Abstract

The iBOSS project at RWTH Aachen—for the development of a modular design for satellites that would enable unmanned on-orbit service and assembly—led to the design of a connecting interface, also able to transfer power and data between the modules; the alignment tolerance for the automated assembly of two modules is however very small, due to the dimension of the components to be aligned.
The aim of this work is to develop an androgynous coupling surface around the interface, to guide the final stage of the approach between two of such interfaces. The coupling between designed surfaces is loose thanks to a peaks-and-valleys design and it gets stricter the closer the surfaces move, up to the point where the mid-planes touch and the surfaces match, to allow the interface's components to align for connection. A secondary function of the surface is to support lateral loads between interfaces, keeping it locked in place without the risk of the power transfer pins being under stress.
The work is divided in three main tasks intertwined with each other: selection of shape and dimensions, analytical analysis of the friction forces that hold the surfaces in place, and Finite Element Analysis of the stresses that develop internally under expected loads.
The final design of the surface manages—under assumptions made to reduce the complexity of the problems at hand—to satisfy the primary function it is designed for: the surfaces couple together with a broader tolerance than that of the interfaces, and alignment between the interfaces themselves is guaranteed within a reasonable temperature gradient between them.
Additionally, the surface withstands lateral loads of the same entity of those the interface has been proofed against: the static friction between surfaces is enough to hold them together, and the acting loads do not result in structural failure of the component.

Keywords:

Coupling interface, Matching tolerances, Finite Elements Method, Static Friction

Ringraziamenti

Per prima cosa voglio ringraziare la mia famiglia: i miei genitori per avermi dato la possibilità di arrivare fin qui, e mie sorelle per non aver assecondato i loro intenti omicidi nei miei confronti.

Ringrazio quindi tutti i compagni che durante gli anni mi hanno concesso di riempire lacune nei miei appunti: se penso a quanto rare siano state le volte in cui mi sia stato chiesto di ricambiare, non posso che elogiarli ancor più (o dubitare della comprensibilità dei miei appunti).

Le amicizie personali hanno poco o nulla a che fare con il percorso formativo, ma è opportuna almeno la menzione dei miei amici, quindi questo è il paragrafo a loro dedicato: agli amici con cui esco regolarmente, a compagni (vecchi e nuovi), a coloro con cui ogni giorno gustavo le pietanze di una delle mense di Padova, e quelli che mi accompagnavano ogni giorno in una corsa in treno in mezzo alle campagne euganee.

Una menzione particolare va infine al periodo più intenso di tutta la mia vita: la mia esperienza Erasmus. È stata la mia prima esperienza fuori casa e, anche se ho interagito meno di quanto speravo con studenti internazionali, è stato un momento particolarmente socievole della mia vita. Ad Aachen ho lasciato un pezzo di me.

...letteralmente. Sono tornato a casa senza appendice.

Marco Bissaro

Contents

List of Figures

List of Tables

1 Introduction

1.1 Objective

The objective of this work is to find an optimal design for a coupling surface (highlighted in red in Figure 1.1) to guide an androgynous interface to the matching position during its approach and connection to another identical interface. The coupling surface is necessary in order to broaden the precision required in the connection manoeuvre: the alignment between one interface's pins and the holes on the other interface requires precision of about 5 mm ([1]), and the aim is to increase it by one order of magnitude. The secondary function of the coupling surface is to prevent lateral shift between the interfaces when a lateral force is applied.

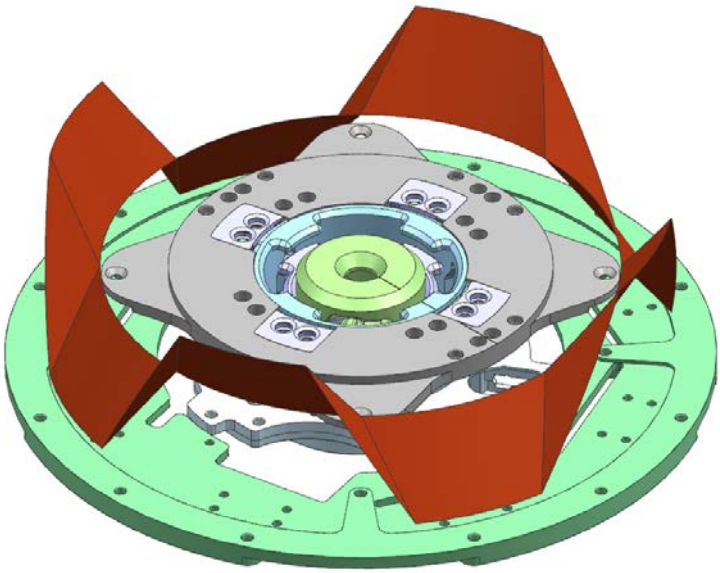

Figure 1.1: Sketch of the coupling surface (in red in the figure) added to the iSSI assembly.

This work originates from the intelligent Building Blocks for On-Orbit Satellite Service and Assembly (iBOSS) project to which the Institute of Structural Mechanics and Lightweight Constructions of RWTH Aachen participated. iBOSS aimed to evaluate the feasibility of the concept of modular satellites and, after carrying out the feasibility evaluation, to develop the actual concept. The development resulted in the design of different components and customer-support services:

- intelligent Building Block (iBLOCK): the module that contains the components, a cube which has a 40 cm side;

- intelligent Space System Interface (iSSI): developed because the modules must be detachable and interchangeable while in orbit and they need power and data transfer between one another;

- intelligent Computer Aided Satellite Design (iCASD): software that helps the customer design a modular satellite, on the base of the characteristics that they choose;

- intelligent Virtual Testbed (VTi) has the aim of enabling the virtualisation of the qualification tests needed before a satellite gets approval for launch, based on previous tests performed on single modules.

The components iBLOCK and iSSI have been manufactured and tested, while most of the other services have to be improved further before the product is commercially available.

Within the iSSI component, one issue left to study is the high accuracy needed for the pairing of two interfaces: in fact, the power-transfer pins align under a 5 mm linear tolerance, which is excessive considering that the iBLOCK side is 40 cm—the resulting relative tolerance is of the order of 1%.
This work focuses on the development of a surface surrounding the interface to solve this issue: with peaks and valleys that fit into each other, the surfaces' coupling broadens the precision required for the interfaces' approach, ensuring the pin-hole alignment in the locking position.
An additional task for the work is to give secondary functions to the coupling surface, such as ensuring its ability to carry lateral loads.

1.2 State of the Art

1.2.1 The iBOSS Project

The iBOSS project, which third and last phase ended in 2018, developed an entire platform around the concept of modular satellites with the capability of on-orbit service and maintenance. The objectives were to contrast the high redundancy required from satellites today and open the possibility of extending the mission duration even in case of fatal failure of one or more subsystems, also to reduce the space pollution generated with each new mission.

The module itself (iBLOCK) is cubic-shaped, with 40 cm edges. The thin-walled tube-shaped rods of the frame are made of a CFRP composite and the walls are made of sandwich panel, where the external walls are made of a CFRP laminate, while the honeycomb structure is made of Aluminium; the nodes that connect the frame are made of an anodised Aluminium, and have holes positioned in such a way that beams can be inserted in the frame's hollow rods to provide additional constraints while the modules are in the rocket's payload fairing, to support the launch loads.
The overall mass of the structure is just above 5 kg, and from evaluations carried out by Scher-van et al. [2], the payload of a module should not exceed 40 kg.
A collection of modules can be assembled into a complete satellite system; if a component was to break, a service satellite could approach the system in orbit and swap the module which holds the broken component with a functioning one, removing the need for redundancy in the system itself.

iSSI (depicted in Figure 1.2) is the interface designed to connect two modules. It is mounted in the middle of a module's sides, and its main scope is to provide mechanical coupling between blocks and the ability to de-couple from either side: this ensures that, in the event of complete failure of one of the two parts, the other would be able to sever the connection and detach, retaining the capability of connecting with a replacement module.

Figure 1.2: iSSI - production model [3].

Additionally, it uses retractable pins and gold-plated coil springs for the power transfer, while data is carried through using optical signals. The interface was created with the following characteristics in mind[4]:

- Androgynous design
- 90 degrees symmetry
- Autonomous locking and releasing
- Retractable mechanism
- Capability of orbital load transfer
- Channels for power and data transfer
- (Optional) capability of heat exchange

1.2.2 Coupling surfaces

Different coupling surfaces can implement various systems to perform different functions. As explained in SENER's technical review[5], there are for example different mechanical locking mechanisms (hook, clamp, carribena and roto-lock), different electrical connection methods (pins, slip rings, tabs and wireless power transmission), numerous commercially abailable standards for data transfer in space, and different thermal transfer methods (heat pipes, fluid loops, water sublimators and pulsating heat pipes). The work also mentions that iBOSS is the prototype closest to a possible final version of such an interface.

The technical review declares spring-pushed tabs as the recommended electrical connection method, while iBOSS uses pins mechanically pushed into holes in the opposite interface. While the electrical pins lock the rotational DoF in the original design, the presence of the coupling surface would take over this role, allowing for the implementation of the spring-pushed tabs instead.

Nasa Docking System The most notable example of an apparatus with the same function as the one engineered in this work is the Nasa Docking System (NDS) [6], seen in Figure 1.3. Its design gave some insight on the issue at hand before the creation of the coupling surface. However, a couple of characteristics of NDS make it incompatible with the requirements set for the coupling surface: lack of a 90° symmetry, and the lack of load-carrying capacity in the design, being that function assigned to a series of hooks placed around the connection ring. Moreover, NDS possesses functions not needed for the aim of this work, or that would overcomplicate the design to the extent that it would get too expensive to produce for the intended application.

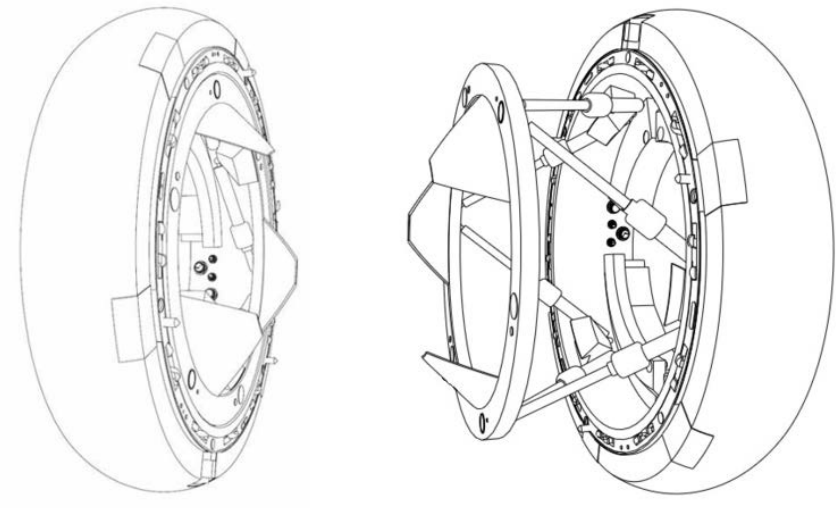

Figure 1.3: The NASA Docking System: an androgynous coupling system that has become standard for docking vehicles to the International Space Station [7].

SIROM One of the currently available interfaces is the Standard Interface for Robotic Manipulation (SIROM) of payload in future space missions, project developed under funding of the EU-funded Horizon 2020 research[8]. SENER is the project's coordinator, and responsible for all phases of the project, from development to manufacturing and integration.

SIROM is a modular reconfigurable system interface with[9]: Mechanical connections between the blocks, Power transmission through electrical connections, Thermal interface for heat transmission, Data transfer through data interfaces. As explained in the previously mentioned technical review [5], SENER integrates:

- Mechanical connection: clamp mechanism
- Electrical connection: standard pins
- Data transfer: SpaceWire and CAN
- Thermal transfer: absent—thermal exchange happens via conduction

This interface is closer to iSSI in design than NDS because its scope is also to connect satellite modules for on-orbit maintenance; it also grants mechanical coupling, and power and data transfer. However, like NDS, its design is not androgynous, nor can it be turned 120°, even if the coupling elements have a 120° symmetry.

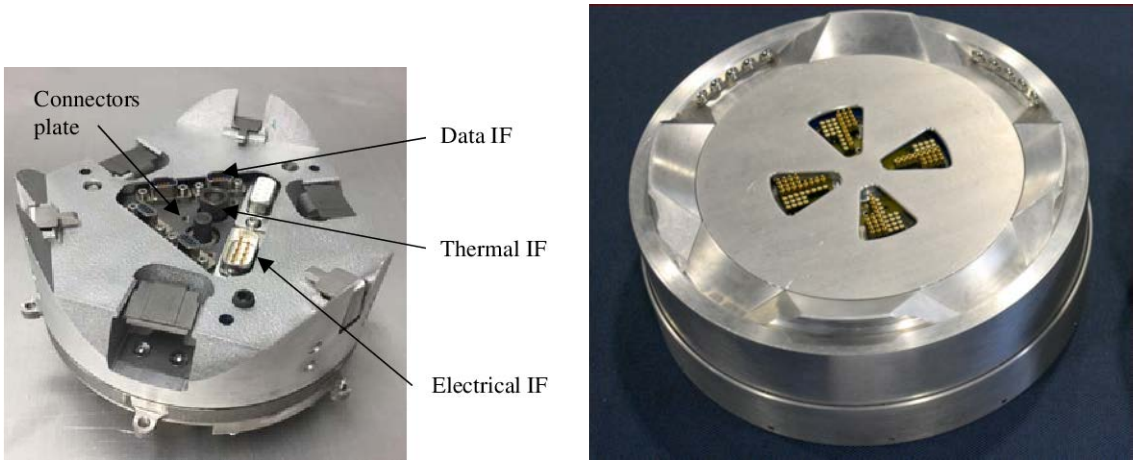

Figure 1.4: The two mentioned interfaces: on the left SIROM [8], on the right HOTDOCK [10].

SpaceApps' HOTDOCK Space Applications Services' HOTDOCK [10] is the design with the most characteristics in common with iSSI. It is the chosen interface for Horizon 2020's Modular Spacecraft Assembly and Reconfiguration (MOSAR) project, whose scope, like iBOSS, was to analyse the feasibility of a modular design for satellites.
HOTDOCK's features include:

- Mechanical interface with a passive connection (carribena)
- Electrical interface for power transfer
- High rate Data transfer
- (optional) Thermal interface, via conduction of fluid coolant

HOTDOCK provides mechanical coupling, power and data transfer, and its design—which is androgynous—includes a form-fit contour to increase the coupling tolerances. The difference with iSSI is that the locking mechanism is found at the extremities of the protruding elements of the form-fit ring. For this reason, this part is integral to the design and its removal is not possible.

1.3 Overview

The work is divided into five chapters, each expanding on a different phase of how the surface design was carried out.
In the second chapter, the problem is described more in detail, and more information is given regarding the environment it must work in and the assumptions taken during the design development;
In the third chapter, the process of the design development is described, along with the reasons behind individual choices;

In the fourth and fifth chapters the methods used to ensure that the surface would be able to exploit its functions are described;
In the sixth chapter, the results of the work are discussed and questioned, and possible improvements are suggested.

2 The problem

The interface has an already defined structure and design that required considerable resources during the iBOSS project. For this reason, the boundary conditions of the problem come from the current structure and capabilities of the iSSI: it is necessary to build the coupling surface around said structure, and to constrain it to the frame and the interface itself, possibly using already existing mounting points.
The interface is compatible with a system of automated assembly, necessary for the operations of on-orbit service. The coupling surface's primary purpose is to aid the connection between interfaces: the inclined surfaces of the component guide the movement towards the alignment position, thanks to larger coupling spaces at the top and edges sloping towards the bottom. The friction developed between the surfaces should be taken into consideration so that it does not impair the relative movement of two surfaces along the plane normal.

Because the components of the iBOSS project operate on orbit, the characteristics of the coupling surface need to be compatible with the space environment and circumstances:

- A space mission commonly lasts between one and two decades, which implies a vast difference between the material conditions at Beginning of Life (BoL) and End of Life (EoL). Because the processes that happen usually bring to a degrade in the material properties over time, the study must ensure successful performances at EoL state for the design;

- Surfaces temperatures in orbit span a substantial interval, because of the absence of contact and convection exchange. The study must take into account the thermal gradient between two surfaces so that it does not impair their coupling.

Material and manufacturing method have to be taken into account, making sure that the overall weight of the piece shall be as small as possible while evaluating the trade-offs needed for a low cost and possibly scalable manufacture. Such characteristics have to be weighed against the capacity of the structure to withstand lateral forces.

2.1 Assumptions and boundary conditions

As aforementioned, the circumstances force the design of the coupling surface to take into account the already existing components of the interface: the coupling surface must use mounting points on the different parts of the interface, and avoid the invasion of volume dedicated to the interface's components. The previous components define therefore unavoidable boundary conditions for the coupling surface's design process.
Additional boundary conditions create linear dependencies between the independent variables of the design, to the extent that one geometric parameter univocally determines the design. Previous evaluations determine that these operations do not restrict excessively the problem.

Load conditions Kortmann et al. [2]—by evaluating the various components that could fit into a 40x40x40 cm space—considered 40 kg as the maximum weight of one module. The value is used in this work as well, to maintain consistency within the development assumptions. A Factor of Safety of 1.5 is taken into account to compensate possible inaccuracies of the models developed.
Moreover, the locking components can withstand a tensile force of up to 6000 N, as found by Kortmann et al. [4]. The information pertains a load scenario where the interfaces pull apart along the direction orthogonal to the plane of connection; the load case considered in this work sees instead the interfaces loaded sideways respect to each other, along the plane of connection.

Temperature difference The conditions of outer space, with no light diffusion nor a convection medium, make it so that the heat exchange can only transmit via contact or radiation, and that different surfaces exposed to objects at different temperatures show a significant difference in temperature. Previous works, notably Schervan et al. [11], take an interval of 200°C around the rest temperature of 20°C. That said, the operative interval for the interface is between -40°C and 70°C; to keep continuity with the studies of thermal deformations, ΔT =200°C is taken into consideration to account for the surfaces' coupling, but in the locking phase ΔT =110°C is used, because of the interface's operative temperature.

2.2 Mounting points

The pre-existing components can not be re-designed in hindsight of the creation of the coupling surface. Because of this, the design process also requires finding mounting points that are compatible with both stated components and the functions that the surface has to carry out. Figure 2.1a shows the design of the iSSI assembly—minus the thermal exchange system, which has to be replaced by the coupling surface. The structure offers mounting points in both the

base-plate and the support ring: the former is at the level of the baseline of the coupling surface, fixed in the inner wall of the sandwich panel, while the latter is at the half-height level.
The base-plate is not an integral part of the interface and is only used to mount it to the back wall of the sandwich panel. Therefore, if the application of the interface is not within the iBOSS project, the base-plate is not essential to the interface's functions. However, the base-plate offers a good starting point for the placement of the surface's mounting points, and it is possible to adapt them for different applications afterwards.

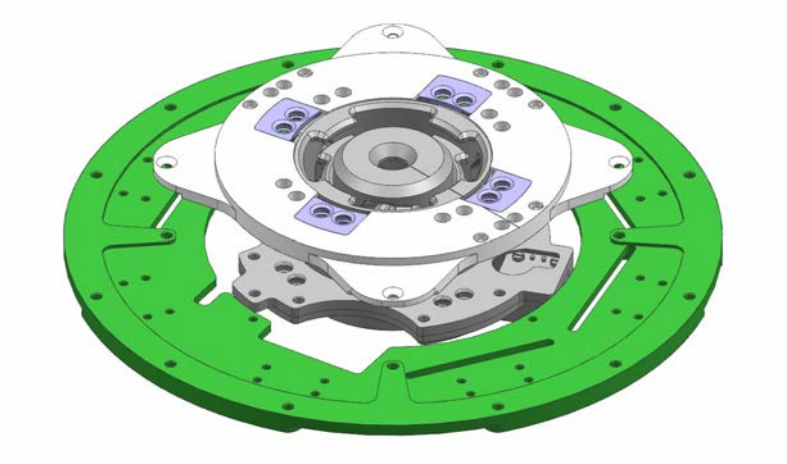

(a) iSSI assembly. In green the base-plate; in white the support ring.

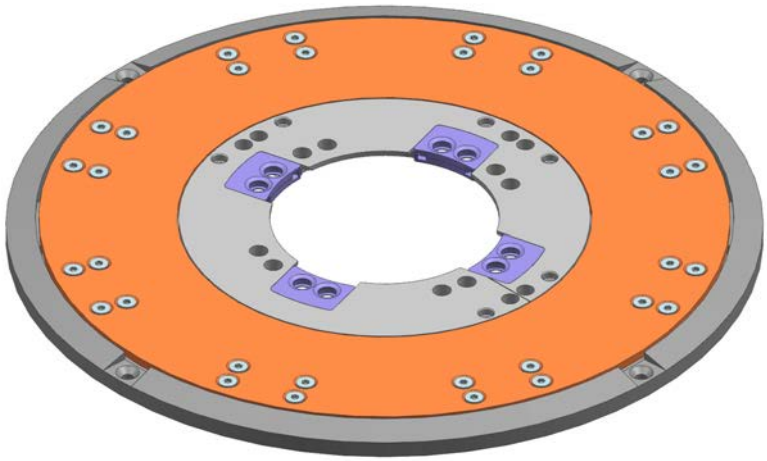

(b) The CAD of thermal interface and support ring.

Figure 2.1: iSSI design assemblies.

The thermal interface's design is connected to the support ring, even if no bolt can be seen in Figure 2.1b where the support ring's mounting flanges are: the thermal interface's external ring has mounting points on 2 mm thick flanges of its own, that connect under the support ring's flanges. However, the role of the coupling surface is different from that of the thermal interface: the latter only touches its counterpart along the connecting plane, and is not subject to heavy loads; the coupling surface is instead supposed to withstand lateral loads, and that requires it

to be firmly fastened to the base. This work makes use of the screw holes in the support ring's flanges to provide for additional mounting points on the inner part than only the ones found on the outer edge of the base-plate. The choice to mount it over the support ring's flanges instead of under them is due to the fact that the inner ring of the component must lie on the connection plane and adding a mounting point under it would complicate the manufacturing—which would void the efforts made to keep it as simple as possible.

The mounting points on the base-plate have no particular encumbrance issue, and they end up in a position more or less centred in the middle of the baseline-level segments of the coupling surface, a position that allows the stresses to distribute evenly without particular stress concentration in one point or direction.
A possible critical point is reached instead in the evaluation on whether the mounting points on the half-height surface are compatible with the final position in the approach of the two interfaces. The middle surfaces are required to touch in the connection plane, and it is of the utmost importance that no parts protrude from the surfaces. This condition prevents full touch between the surfaces and, therefore, connection or alignment between the interfaces.
This problem can be circumvented by using countersunk flat-head screws as fasteners and placing the screw hole in a small recess in the surface (depth of 0.5 mm) as a countermeasure against any possible issue given by the manufacture tolerances of both surface and fasteners. This last feature is not essential, and can be left out if the build tolerances of the screw heads guarantee that no component protrude from the matching surface; one alternative to a cylindrical recess is to adopt a deeper conical countersink in the surface.

2.3 Alignment

Alignment is the main task of the coupling surface—it is only natural that the first and essential requirements to satisfy are those related to this aspect.
The geometry of the surface acts a significant part in the first phase of the approach when the two interfaces are still far from each other: a broader coupling space between the surfaces allows for looser tolerances required from the assembling device. The tolerances of the piece must be taken into account when reaching the last phase of the approach, for the alignment requires high accuracy to align some of the interface components: the pins used for power transmission have to be pushed into holes in the opposite interface.
The alignment conditions must also be verified in the worst-case scenario, defined as the state where the surfaces are subject to a $\Delta T = 110°\mathrm{C}$, the maximum span of the interface's operative temperature interval.

2.4 Materials and manufacturing

Material choice and manufacturing choice are strictly connected by a series of properties that the structure assumes as a consequence: they entangle in the final values of failure load and structural weight.

2.4.1 Materials

The material choice is the most influential in terms of mechanical, thermal and surface properties, and heavily influences the weight of the part, for a piece of known volume and shape.
The choice of the material falls among the different materials mainly used in aerospace: metals are the first choice because of their excellent mechanical properties and durability, even if their density is higher than most of the materials available today; polymers, although lighter, are preferably avoided due to their tendency to get damaged by the high-intensity radiation—especially UV, not absorbed by the Ozone layer—and to lose mass because of material outgassing in the vacuum of space.
The possibility of using a CFRP laminate has been discarded in the early stages of the evaluation because of its complicated and expensive manufacturing, and because of the anisotropy of its mechanical properties: the surface geometry is complicated enough in itself, and an anisotropic material would add preferential paths for the stresses to follow. The FE simulation of the load conditions would not be particularly complicated, but selecting the order of the laminates disposition aforehand would be complicated by a considerable amount of degrees of freedom to the problem.

Aluminium is the metal chosen for this application because of the excellent ratio between its density and mechanical properties. In particular, two alloys were considered: Al7075—the most diffused alloy in aerospace applications—and Al6061 for its excellent thermal conduction properties, which would be of use in the chance that the coupling surface took the additional function of heat exchange interface. In the end, Al7075 revealed more fitting for the evaluations of this work, which main focus is on mechanical performances: Al6061 appears to be more rigid and have a more brittle behaviour, with yield and break stresses of about half the ones of Al7075. In Table 2.1 can be found the properties used in this work[12].

Friction Friction between the surfaces may influence the performance of the component in opposite ways: a high friction coefficient hinders the approach of the two surfaces by posing resistance to their sliding motion, while a low friction coefficient causes the surfaces to slip when under a lateral load, which is then transferred wholly to the locking mechanism.

Property	**Value**
Young Modulus E	71.7 [GPa]
Shear Modulus G	26.9 [GPa]
Poisson Ratio	0.3
Yield failure stress	517 [MPa]
Ultimate failure stress	568 [MPa]
Coefficient of thermal expansion @20°C	23 $[\mu m/(m*K)]$
Coefficient of thermal expansion @200°C	24.5 $[\mu m/(m*K)]$
Density	2810 $[kg/m^3]$

Table 2.1: Respectively Mechanical, Thermal and material properties of Al7075 used in this study.

The surface state of the material influences the friction force between two surfaces; in the case of aluminium, the surface oxidation that happens because of the highly reactive atomic oxygen (ATOX) in the ionosphere causes a layer of aluminium oxide (Al_2O_3) to form on the surface of any component made of aluminium. This phenomenon is beneficial for the aluminium parts, as it stops the oxidation to this first layer, and does not degrade the material further.
The friction coefficient between the surfaces can be considered as aluminium on aluminium for an operation performed on earth, where the surface has not yet been exposed to ATOX, or as aluminium oxide on aluminium oxide, for an operation performed on orbit. For the reference on the values used, see the work of Buckley et al. [13]: tests on the friction between two aluminium oxide components in different conditions in vacuum show different behaviours for different conditions, in particular, the crystal orientation; nonetheless, because the formation of the oxide in the ionosphere is not a controlled phenomenon, the assumption taken is that the crystal does not have a preferential direction of growth. The value of the friction coefficient obtained by Buckley et al. [13] in the case of polycrystalline aluminium oxide is $\alpha = 0.78$. Instead, in case of non-oxidized aluminium, the coefficient of friction falls in the [1.05;1.35] interval (data common between different online resources and ultimately confirmed by [14]).
The iSSI components are coated with a diamond-like surface treatment [1], which decreases the friction coefficient to less than 0.1.

After all these considerations, it should be pointed out that the most critical phase where a lateral force is exerted between the interfaces is during the satellite assembly on earth when an automated apparatus manoeuvres the module: during the launch, the assumption is that the modules are fixed to the payload fairing using beams passing through the frame hollow rods.
The consequence of this assumption is that the coefficient to be used in the analysis of the load supported by static friction is the one between $Al - Al$, not $Al_2O_3 - Al_2O_3$. In case the coupling surface is coated as the other components, the coefficient of friction becomes extremely low, and static friction does not hold the lateral loads.

2.4.2 Manufacturing

The choice between a solid piece and a metal sheet lies again on the possibility to obtain a lighter structure while maintaining the required functionalities. Having a monolithic piece, in this case, has two disadvantages: first, the volume occupied would intersect with the volume assigned to the engine placement and second, the manufacturing method required is machining, which is quite costly and slow.
The engine is one of the few components the placement of which is extremely challenging to change: its dimensions, relatively to the interface, are so big that it can not be closer to the interface's axis. For this reason, it would require an additional cut-out from the metal block, and this would increase costs, manufacturing time and complexity.

On the other hand, a piece obtained from a metal sheet is lighter, occupies little volume and has the added value of secure and scalable manufacturing by deep-drawing technology. Because, as will be seen in Chapter 5 the stresses on the surface studied as a metal sheet are proved not to be too high for the material to sustain, this is the chosen form factor for the design.

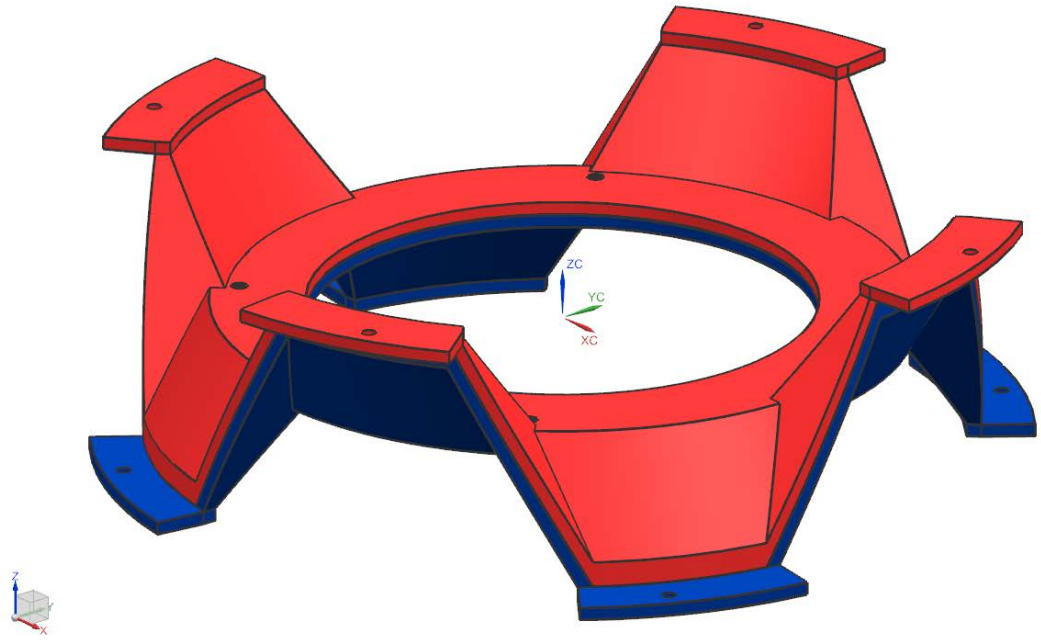

Figure 2.2: The matching position of the coupling surfaces.

3 Design

3.1 Idealized geometry

3.1.1 Reference System

The definition of a Reference System in the space containing the surface is the first step necessary to describe the geometry of the coupling surface.
Cylindrical coordinates are used, with the origin in the centre of the contact surface. The three coordinates highlighted in red in Figure 3.1 are: radial direction (linear coordinate ρ), circumferential direction (angular coordinate θ), and vertical direction (z).
The zeros of the coordinate system are the origin O for the ρ coordinate; x-axis for the θ coordinate; the plane of the upper surface of the support ring for the z coordinate.

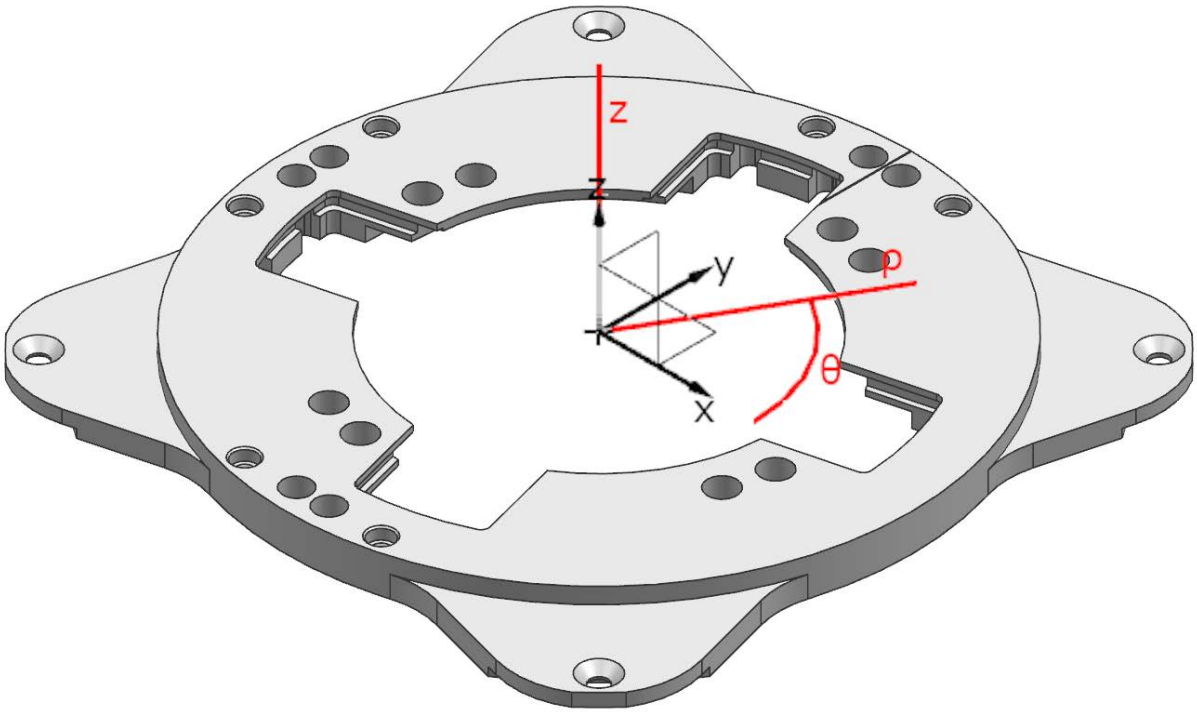

Figure 3.1: Position of the Reference System with respect to the support ring.

3.1.2 Outer edge

The design of the coupling surface has to be built around two specific requirements:

- androgyny: requires a single piece to have both male and female features—taken two random clones of the same design, they must match.
- 90 degrees symmetry: the interfaces must be able to connect even if rotated by 90 degrees.

The first point guides the design choice to a shape that follows a sinusoidal curve along the circumference. The second point requires the repetition of a sine period on each quadrant so that the function it follows is:

$$t = t_{max} * sin(4\theta) \tag{3.1}$$

The t_{max} value is defined as the highest value the geometry can reach in the negative thickness—obtained by the boundaries created by the pre-existing geometry, which defines the lowest point the coupling surface can reach into the thickness of the interface. The highest point is mirrored respect to the interface's upper plane, to maintain the condition of androgyny.

Rotating the curve by 180° around the x or y-axis, the result is always the starting curve. This condition is satisfied also for 90° rotations around the z-axis.
The translation of the phenomenon in the engineering application is that, when two surfaces are facing each other, the positive (convex, or male) part of one surface always meets the negative (concave, or female) part of the other.

Because of manufacturing feasibility and study ease, the curve shape assumed along the circumference is not a proper sine function, but a broken line, composed of straight segments. Additionally, the selected manufacturing choice for this work is deep drawing, which creates more precise sharp angles than wide curves, because of the elastic behaviour of metals and the more drastic plastic transformation implied in the former.
The design variable in this work is γ, half the angular amplitude of the inclined curves along the circumference. Around the points where $sin(\theta) = \pm 1$, for a certain width (whose amplitude is $\beta = \pi/4 - \gamma$), the curve stays at constant height $t = \pm t_{max}$; these segments are connected by slopes with a constant inclination, of width 2γ.

Using a broken line as a border has a positive side-effect on the secondary function of the surface—to carry lateral loads. In fact, this design increases the average angle between the slope's surface and the xy plane. The higher this angle, the more the surface is normal to the lateral forces, for they are defined as laying on said plane.
In a pure sine function, the tangent—which defines the angle between the curve and the xy plane—reaches its maximum value (45°) in the middle of the slopes, and gradually decreases to 0° towards the extremities of the slope. In a broken line the tangent keeps instead constant for the entire slope: from a 45° inclination of the slopes, this guarantees that the tangent be higher than the average tangent in the pure sine function, which is certainly lower than 45°.
The broken-line function becomes:

$$\begin{cases} t = \frac{\theta}{\gamma/2} * t_{max} & for \quad 0 < \theta \leq \frac{\gamma}{2} \\ t = t_{max} & for \quad \frac{\gamma}{2} < \theta \leq \frac{\pi}{4} - \frac{\gamma}{2} \\ t = (1/2 + \frac{\pi/4+\gamma/2-\theta}{\gamma}) * (-2t_{max}) & for \quad \frac{\pi}{4} - \frac{\gamma}{2} < \theta \leq \frac{\pi}{4} + \frac{\gamma}{2} \\ t = (-t_{max}) & for \quad \frac{\pi}{4} + \frac{\gamma}{2} < \theta \leq \frac{\pi}{2} - \frac{\gamma}{2} \\ t = (1/2 + \frac{\pi/2+\gamma/2-\theta}{\gamma}) * 2t_{max} & for \quad \frac{\pi}{2} - \frac{\gamma}{2} < \theta \leq \frac{\pi}{2} \end{cases}$$

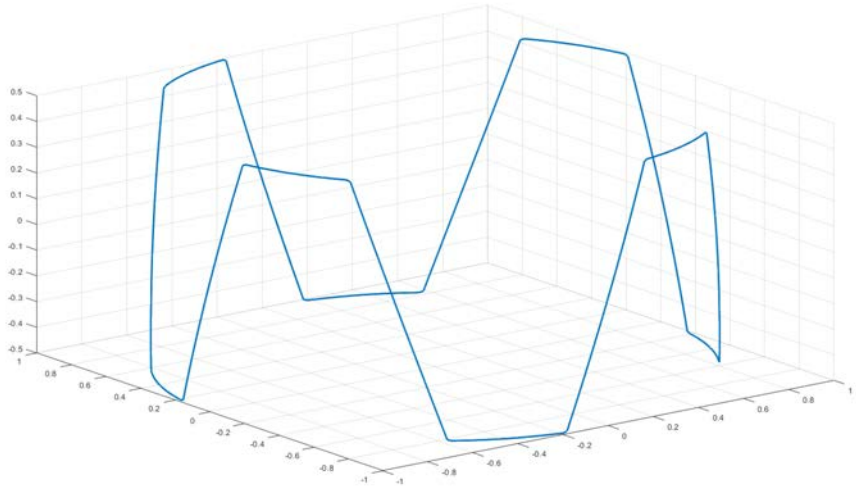

(a) The line traced by the outer border of the coupling surface geometry.

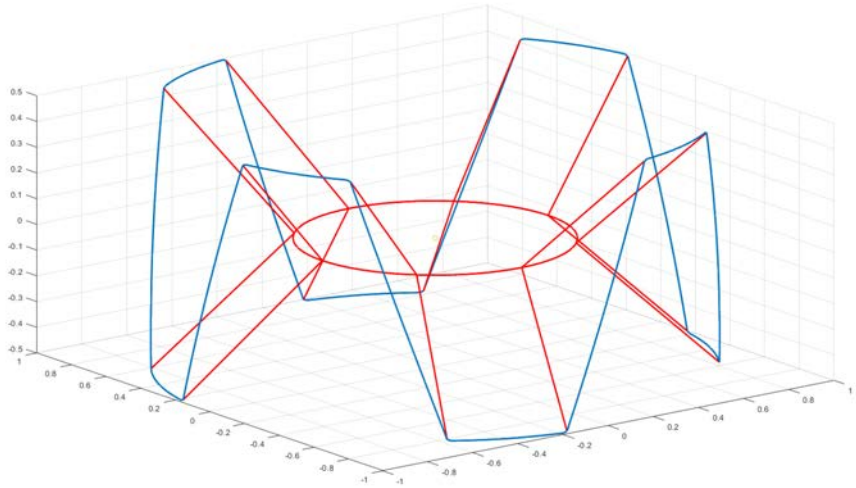

(b) Idealized geometry of the coupling surface.

Figure 3.2: The lines that characterise the idealized geometry, traced in MATLAB.

3.1.3 Faces

The inner edge of the coupling surface coincides by design necessity with the outer border of the interface, which lies on the plane at half the thickness of the whole geometry: connecting the inner edge to the outer edge requires a slope in the radial direction. The same inclination angle is assigned to the slope in the radial direction and the circumferential direction to reduce the design possibilities; otherwise, this would become an additional design variable.

The internal border follows a circumference on the *xy* plane. A straight line connects each breaking point of the outer border to a point on the circumference, in such a way that the borders at constant height are sides of pseudo-quadrilaterals. At the same time, the slopes are borders of pseudo-triangles (so-called because the figures formed are not polygons: in fact the sides that lay on the external border are curvilineal). The meeting points of the lines on the internal border are at $\theta = k * pi/4 \quad (for\ k = 0,\ldots,7)$, also coordinates of the meeting points between slopes and *xy* plane.

3.2 CAD Model

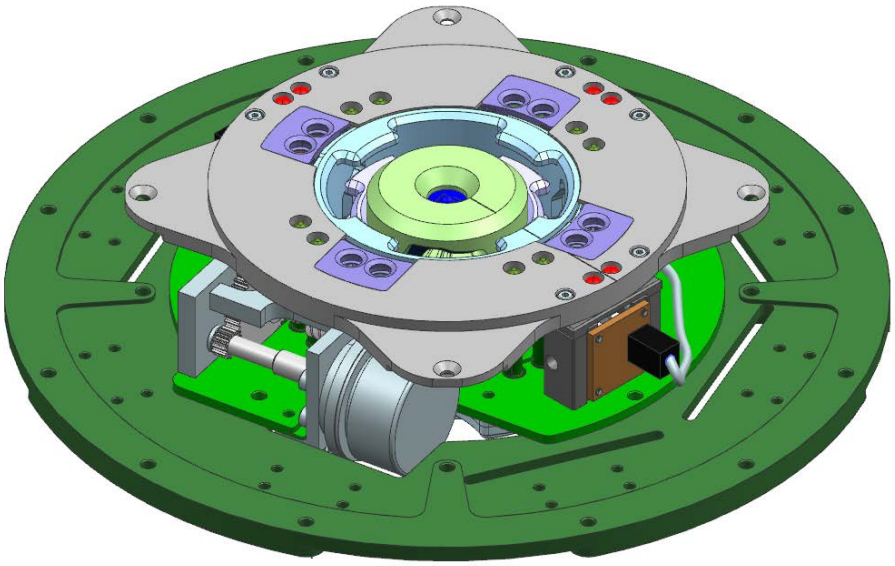

Figure 3.3: The iSSI assembly complete of electrical components.

In Figure 3.3 is represented the iSSI assembly complete of electrical components, included the motor. The base-plate offers twelve mounting points, and the support ring offers four; the motor occupies a volume that goes outside the boundaries created by the outer diameter of the support ring but stays within the diameter of the support ring's mounting flanges. Furthermore, there is

Property	Value
Minimum distance between α and η	$\delta z = 3 \times 10^{-3} m$
Minimum distance between υ and α	$\Delta z = 2.99 \times 10^{-2} m$
Support ring outer diameter	$D_{out,ring} = 1.19 \times 10^{-1} m$
Support ring mounting flanges outer diameter	$D_{out,flange} = 8 \times 10^{-2} m$
Base-plate outer diameter	$D_{out,base} = 1.1 \times 10^{-1} m$

Table 3.1: α: Upper surface of mounting point flanges; η: Upper surface of support ring (also interfaces contact surface); υ: Upper surface of base-plate.

a small gap between the mounting flanges' upper surface and the support ring's upper surface—which lies on the interfaces' connection plane. These are the main points around the coupling surface's creation.
In Table 3.1 can be found a list of some measurements from the iSSI assembly used in the process of building the design.

The small gap between the connection plane and the upper surface of the mounting flanges of the support ring (minimum distance between α and η) is the thickness of the metal sheet: the maximum value permitted by the interface design, to obtain the maximum mechanical performances.
A planar ring with inner diameter $D_{out,ring}$ and outer diameter $D_{out,flange}$ connects to the inner edge of the coupling surface, so that $D_{out,flange}$ is the inner diameter of the coupling surface(as idealized in Section 3.1); $R_{out,base} = D_{out,base}/2$ is used as upper limit for the coupling surface's outer radius; the total height of the coupling surface is $h = 2 * \Delta z$, as previously stated, assuming the distance between υ and α as the thickness of the interface.

To these dimensions, some corrections are made to ensure mounting capability even in the occasion of manufacturing defects: the inner border has an inner radius of $R_{in,coupling} = R_{out,ring} + 1\ mm$, and the height is $h_{tot} = 2 * \Delta z - 0.1\ mm$. The latter being one order of magnitude smaller than the former because the contact between the interfaces is a condition for a successful connection.

The final model has a volume of 92639.435 mm^3: if the material used is Al7075, using the density in Table 2.1, the mass of the component results in 0.260 kg.

3.2.1 Procedure

Two major phases define the procedure that allows building the final model in the CAD software Siemens NX 12.0: first, the creation of the idealised coupling surface, and its conversion to a separate file; secondly, the use of the previously created file to generate a more detailed component, and the addition to the model of surfaces where to place the mounting points.

Coupling Surface

1. A sketch on the *yz* plane, of an isosceles triangle with the vertex at $R = r_{in,coupling}$ and base—of length $l = h_{tot}$, parallel to z-axis—at $R = R_{out,coupling}$ is revolved around the z-axis;

2. On the upper and lower edges of the revolution solid, the start and endpoints of the constant height segments are marked, and in the inner border are marked all points corresponding to $\theta = k * \pi/4$;

3. Using the tool *Curve on surface*, the curves that connect those points are created;

4. Using the tool *Fill surface*, the triangular surfaces of the coupling surface are created, selecting the curves of point 3 as edges of the surfaces.

5. Using the tool *Split body*, the solid obtained with the revolution at point 1 is split into eight different bodies.

To speed up the process points number 2 through 4 can be executed in only one quadrant, and patterned circularly with the tool *Pattern feature*.
The model just created contains all the surfaces necessary for the coupling surface, and the body split shows in a way how two clone surfaces fit into each other.
This model does not allow to remove from the model isolated parts obtained from the *Body split* function, so the entire geometry is exported as a Parasolid file. It is then imported back in a new Siemens NX 12.0 model, an operation that determines the split of the whole process in two phases.

Final model

1. Half of the solid bodies are removed from the model so that four separated bodies remain (see Figure in Appendix C).

2. To connect them, a sketch on the *yz* plane—of a rectangular trapezoid with the perpendicular side at $\rho = R_{out,ring} + 1\ mm$, vertex of the minor base at $\rho = R_{out,flange}$ and vertex of the major base at $\rho = R_{out,coupling}$—is revolved around the z-axis;

3. A *Boolean add* is performed between all the bodies that are in the model

4. The *Shell* tool is used to remove the bottom, inner and outer surfaces, leaving a thickness of 3 mm, as previously stated;

5. Flanges are added to the lowest segments of the interface, to serve as mounting points bolted to the base-plate. This operation is done by extruding by 3 mm a sketch of a ring sector as large as the constant height segment and with outer radius $R = R_{out,base}$;

6. Holes are added to the flanges, in the points that coincide with the holes in the base-plate;

7. Holes slightly larger than the head of a countersunk screw of the type used in the iSSI assembly are made on the inner ring, with a depth of a fraction of a millimetre, in the same position as the mounting points on the support ring flanges;

8. Countersunk screw holes are added, starting from the bottom of the hollows just created.

In point 5 it is important to extrude in the opposite direction to where the body develops because the geometry of the body is essential to the function of alignment that the coupling surface has to carry out. Points from 5 to the end can be sped up by using the *Pattern feature* tool after performing them in only one quadrant.

The characteristics of the obtained piece are shown in Table 3.2. The values of the coupling surface outer radius $r_{ps,out}$, the angle between slope surfaces and vertical axis γ, and the slopes' circular sector angle δ all come from calculations described in Chapter 4: as previously stated, the two processes are deeply intertwined, in that the boundary conditions for the parametrisation have to be taken by the iSSI CAD model, and the parametrisation results give the dimensions to use to build the CAD model. The parametrisation gives many design dimensions from which to choose. The $\delta = 20.02°$ parameter value choice is made using an arbitrary trade-off: the amount of pre-tension required from the locking mechanism is on the lower side of the curve, and the alignment tolerances are kept quite wide. The specific value is picked on the basis that $\gamma = 60.32°$ is particularly close to the notable value of $60° = \pi/3$.

Property	**Value**
Inner radius	$r_{in} = 59.50\ mm$
Inner ring outer radius	$r_{ps,in} = 89.50\ mm$
coupling surface outer radius	$r_{ps,out} = 97.52\ mm$
Angle between slope surfaces and vertical	$\gamma = 60.32°$
Slopes circular sector angle	$\delta = 20.02°$
Support flanges outer radius	$r_{out} = 110.00\ mm$
Height	$h = 59.70mm$
Wall thickness	$t = 3\ mm$
Al7075 density	$\rho_{Al7075} = 2810 kg/m^3$
Solid volume	$Vol = 9.3 \times 10^{-5} m^3$
Component mass	$M_tot = 261.33g$

Table 3.2: Geometrical description of the solid body.

In the Figures in Appendix C are shown the steps described in Section 3.2.1, that come together to the final build of the coupling surface CAD model.

3.2.2 Alignment

The obtained design allows correct coupling between the two surfaces, even in the event of misalignment of about 3 cm (linear), or 20° (angular), as seen in Figure 3.4. These are the two main misalignment cases, which is possible to combine to obtain other "hybrid" cases. The diagonal approach is possible up to a 30° inclination between the trajectory and the axis. This might prove critical in case a module with interfaces on adjacent sides should be connected to both interfaces: the connection requires a 45° trajectory, which would be hindered by the coupling surface's protrusions.

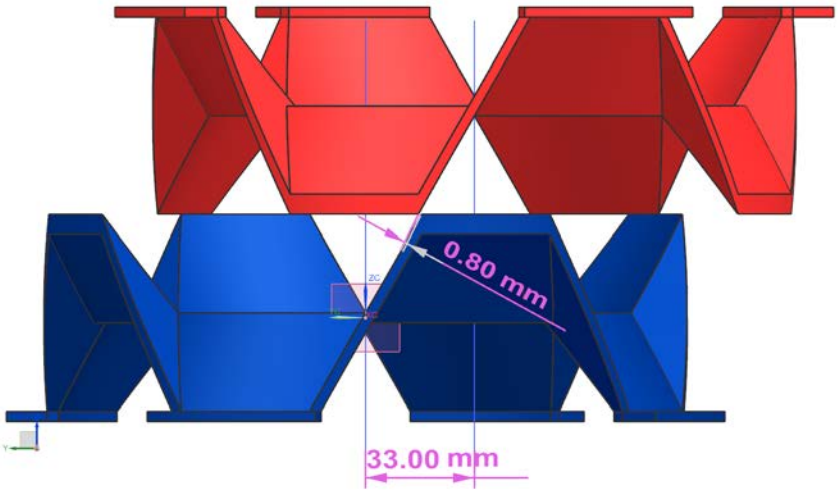

(a) Linear misalignment 33 mm.

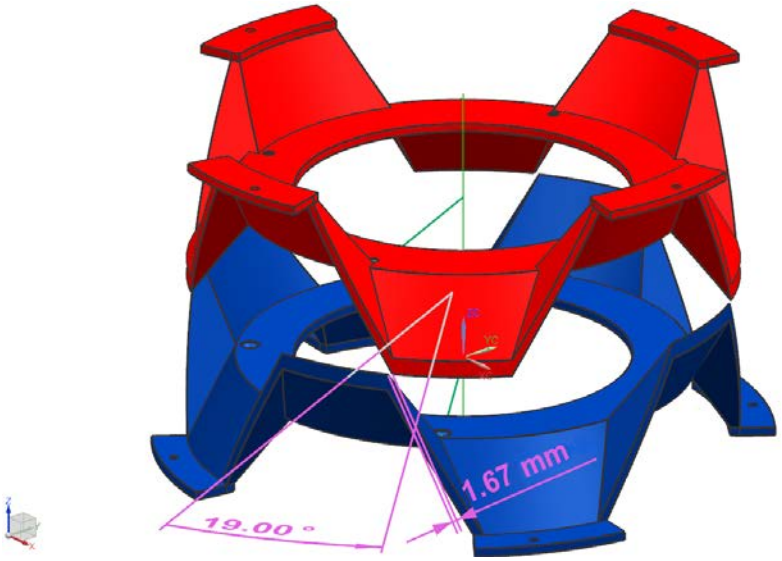

(b) Angular misalignment 19°.

Figure 3.4: Linear and angular misalignment between coupling surfaces.

3.3 Manufacturing

The manufacturing method chosen for piece production is a form of sheet bending: deep-drawing. The main advantage of a component in the form of a metal sheet is that its production is far more rapid than if it were a solid piece: metal sheets can be bent with a relatively low effort to make them take the desired shape, while a monolithic component needs die-casting, and a generic-shaped piece has to be machined to obtain the desired shape. Machining is more costly than metal sheet bending in the context of large scale production and more suitable for complex parts; die-casting is a slower process overall, and more suited for monolithic components, which have the disadvantage of carrying more mass than a sheet metal component.

The sheet metal area required for this manufacturing method is the area of a circumference that has for radius the sum of the curves traced in Figure 3.5. The total radius becomes: r_{sheet} =34.359 mm+ 80.5 mm+ 12.484 mm= 127.343 mm.

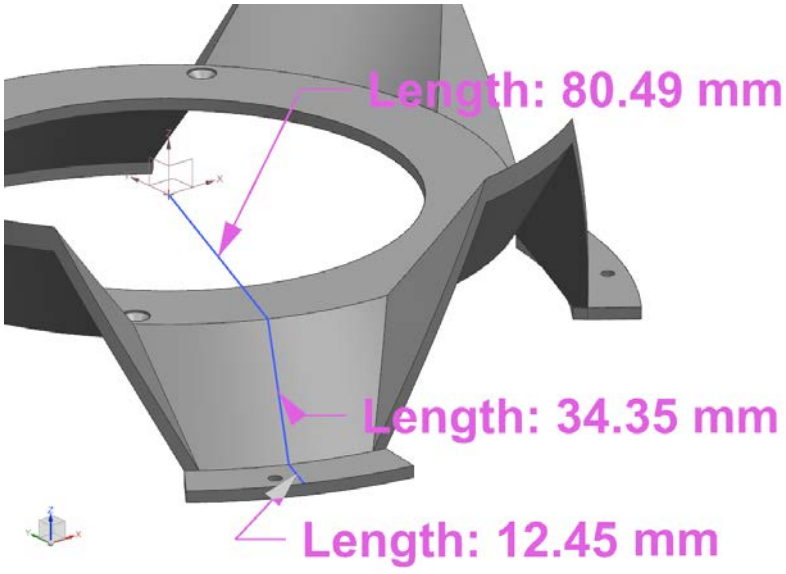

Figure 3.5: Concatenation of the curves that follow the radial profile of the coupling surface.

The main issue that could be encountered with this manufacturing method is that the metal is stretched along the circumferential direction when the slopes are created: this operation—according to the mathematical laws, under the assumption that the volume of the material remains constant—reduces the thickness of the sheet farther from the centre, where the elongation is the highest. The cause is in the difference between the area as a planar surface, and after it develops in the third dimension: the material farther from the centre is stretched more. Such an event could produce further complications: higher stresses in certain zones of the material, and possibly tears in the metal sheet, in the case it is stretched too much. The stretch of the material is non-linear and depends on the manufacturing parameters, which are unknown at the time. Therefore the manufacturing of the piece is to be analysed more in-depth.

3.4 Tolerances

The condition that ensures the alignment of the surfaces in all cases is their alignment in the worst-case scenario. In this study, the worst-case scenario selected is a temperature difference between the two interfaces, which can occur if one surface sees the Sun and the other only sees the black sky or some form of planet albedo. Because the temperature operative interval of the interface is between -40°C and 70°C, 110 K is the temperature difference assumed for the worst-case scenario, assuming that the two interfaces are in thermal equilibrium with the respective coupling surfaces. The 200 K temperature difference mentioned in Chapter 2 is not relevant for this work.
The thermal properties of the Al7075 alloy can be found in Table 2.1: the value of the Coefficient of thermal expansion used is the one at 20 °C because the average temperature range of a component in orbit is around this value.

The law of linear thermal expansion is stated as follows:

$$\frac{\Delta L}{L_0} = \alpha_{T0} * (T - T_0) \tag{3.2}$$

$$= \alpha * \Delta T \tag{3.3}$$

Assuming ΔT =110 K as previously stated, and $\alpha = 23.6 \mu m/m\ K$, the linear deformation is:

$$\frac{\Delta L}{L_0} = 2.596 \times 10^{-3} \tag{3.4}$$

The material deforms by 0.26% of its dimension under such thermal stress.

The height of the coupling surface is 60 mm. When one component grows respect to the other, its height grows as well: in this case, the tips of the protruding parts touch the base of the other coupling surface before the two surfaces can meet, preventing the surfaces from touching extensively. This gap is, in the worst-case scenario:

$$\delta_z = 30\ mm * 2.596 \times 10^{-3} \tag{3.5}$$

$$= 0.078\ mm \tag{3.6}$$

The calculation of radial misalignment requires the inner radius of the coupling surface, which—not counting the inner ring—is 80.5 mm. The axis of one power transmission pin is at a distance of 40 mm from the interface axis. If the inner borders of the slopes are touching at the point farthest from the pin's axis, the misalignment between pin and hole axes is:

$$\delta\rho = (80.5\ mm + 40\ mm) * 2.596 \times 10^{-3} \tag{3.7}$$
$$= 0.313\ mm \tag{3.8}$$

The power-conducting pins have a diameter d_{pin} =5 mm, while the holes they are ejected into have a diameter $d_{pinhole}$ =5.4 mm [15].
The alignment tolerance for the iSSI interface—assumed as displacement from the exact alignment position, where pin and hole are coaxial—is δr_{pin} =0.2 mm. The pins are designed to be electrically insulated in every part of their length but the area where they are supposed to make contact with the coiled springs, to be in working condition even if touching the walls of the holes.

However, because the pin is flexible, its conic end guides its entrance in the hole, guided by the countersink. This design broadens the required tolerance: for the pin-hole coupling, in this case, the displacement must be smaller than the difference between pin and hole diameters (δd_{pin} =0.4 mm). The misalignment causes the intersection of the holes' areas to take a shape that resembles an ellipse (Figure 3.6 shows the described behaviour), of which the minor axis is $a = d_{hole} - \Delta x$: this physically prevents the pin from entering the holes' intersection if $\Delta x > \delta d_{pin}$. Taking into account the misalignment due to thermal deformation, the tolerances required from the surface's manufacturing in the radial direction is equal to $\delta d_{pin} - \delta\rho$ =0.0872 mm.

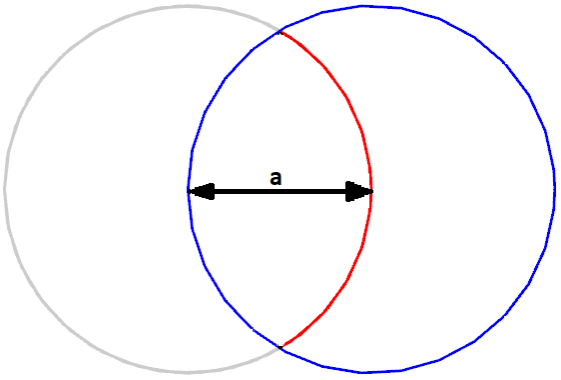

Figure 3.6: Sketch of an intersection of two holes.

Because the mechanical alignment function of the electrical pins is carried out by the coupling surface, the pins ejection can be performed after the interfaces have mechanically locked. The close contact of the two surfaces increases the thermal exchange between them, and in some

time their temperatures converge to the same value. At this point, the pin-hole alignment is determined solely by the manufacturing tolerances, which can be set to the previously calculated value of $\delta d_{pin} = 0.4$ mm.

4 Parameter-dependant behaviour

The first physical study of the design carried out during the work is a simplified analytical model of the friction between connected coupling surfaces, in the event of a shearing force acting along the plane of connection. In this case, the coupling surface has to withstand lateral forces: because no surface is orthogonal to the plane, the resistance is granted by the friction that develops between the inclined surfaces, while the two pieces are being held together by the interface locking mechanism.

Since this phase aims to be an analytical study—less complicated than a numerical simulation—it was exploited to find the optimal geometric parameters to use in the design to be tested within a FE environment: cycling through values of a parameter, the shape of the coupling surface flattens or straightens, with the amplitude of the slopes varying accordingly; with it varies the coupling tolerance of the coupling surface—that coincides with the tips' allowed misalignment—and the area of the inclined surfaces projections on the vertical planes.

4.1 Geometry parametrization

Boundary conditions and assumptions allow the geometry of the coupling surface to have linearly dependant dimensions so that only one independent parameter could be changed to obtain a different geometry. The dimension taken as the independent variable is γ.

In Figure 4.1 are represented the geometric dimensions of the coupling surface; following are defined the mathematical relations between them, and is pointed out when the dependence is given by an aimed assumption or a boundary condition generated by the preexisting geometry. The mathematical relations between shape and meeting tolerances will also be determined here. First, the laws that bind all the dimensions to the variable γ:

$$tan(\delta_\theta) = \frac{H/2}{2R_e sin(\gamma/2)} \tag{4.1}$$

$$tan(\delta_r) = \frac{H/2}{R_{out} - R_{in}} \tag{4.2}$$

$$R_{ext} = \frac{R_{int}}{1 - 2sin(\gamma/2)} \tag{4.3}$$

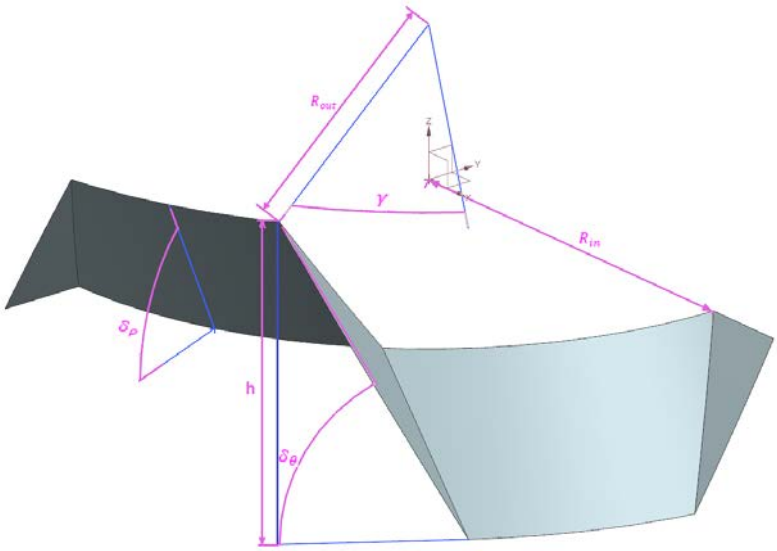

Figure 4.1: One quadrant of the coupling surface, on which are highligted the geometric dimensions.

The relations between geometrical dimensions and meeting tolerances:

$$\Delta x_{max} = 2R_{ext} sin(\gamma/2) \tag{4.4}$$

$$\Delta\theta_{max} = \gamma \tag{4.5}$$

Where Δx_{max} is the tolerance for linear misalignment, and $\Delta\theta_{max}$ is the tolerance for angular misalignment. Combining 4.3, 4.5 and 4.4 we obtain the relation between the two approach tolerances to determine which of the two is more strict; having a mathematical relation between the two tolerances allows to have only one boundary condition for the problem, fixed on the stricter condition.

$$\gamma_{min} = 2arcsin\left(\frac{1}{2(1+\frac{R_{in}}{x_{tol}})}\right) \tag{4.6}$$

Finally, the external radius will be univocally determined by γ thanks to the condition $\delta_r = \delta_\theta$, and because of this, combining equations 4.5 and 4.4:

$$R_{ext} = \frac{R_{in}}{1-2sin(\gamma/2)} \tag{4.7}$$

In addition to this, Equation 4.3 gives an upper limit to γ because the external radius will have an upper limit, given by the outer radius of the base-plate.

4.2 Friction model

Because no surface is normal to the interface plane, any force applied along this plane will be supported by the static friction between the inclined surfaces. The forces are split into components directed with the axes, and each direction is analysed on its own. Finally, they are combined after the necessary calculations.

The problem is stated as follows: given a pre-determined tangential force, find the minimum compression force to apply to the surfaces so that they will not slide on each other.
The maximum normal load withstandable by the interface is related both to the tangential force—because a 90-degree rotation around an axis of the horizontal plane transforms the load from normal to tangential, and to the compression force—because it is the force generated by the locking mechanism that keeps the coupling surfaces together. The choice of using the tangential force as input and the normal force as output was taken due to the linearity of the algebra involved.

4.2.1 Workflow

1. The faces are projected onto the three cartesian planes, and projections' areas are calculated;
2. The components of the force acting along the *xy* plane are distributed among all the faces' projections;
3. For each face, the resulting components are projected on the plane of the face;
4. The laws of mechanics are applied to find the failure condition of the static friction along each direction;
5. The components are combined to find the resultant;
6. The area projection of the face on the *xy* plane is used to find the total normal force from the fraction of normal force acting on the face;
7. The maximum among all the obtained forces is assumed as the failure condition of the static friction.

In step 2, the fraction of the force component acting on a face is determined by the area projected on the plane normal to the component itself. Moreover, the last step is performed on the assumption that when the face holding most of the static friction fails, the force to sustain is spread amongst all the other faces. The force on each face increases in magnitude, and the static friction fails consequently on them as well.

4.3 Calculating the forces

Because the coupling surface benefits of 90-degrees symmetry, the operations need not be performed on all its faces, but only on a quadrant of the plane. To obtain the results on other quadrants, three 90-degrees subsequent rotations can be performed by multiplying the force vector $F = [F_x;\ F_y]$ by the rotation matrix $\left[\begin{smallmatrix} 0 & 1 \\ -1 & 0 \end{smallmatrix}\right]$.

Only the exterior of the surface opposes resistance to the applied force, which means that only the faces which normal vector (pointing outside) has a direction opposite to the force direction oppose any resistance to it. Some faces contain one of the horizontal axes, and therefore their projection on the plane orthogonal to that direction is empty. These conditions combined make so that different faces support the force applied to the system in different ways.
For each face, the equilibrium of forces comes from the equation of Friction (D) and the tangential component of the applied force (T):

$$D = \mu(P_n + F_n) \tag{4.8}$$
$$T = F_t - P_t \tag{4.9}$$

The components along x and y need to be calculated on each face, while the z component of the force always projects on the faces with the following law:

$$F_t = F_z sin\delta \tag{4.10}$$
$$F_n = F_z cos\delta \tag{4.11}$$

4.3.1 Positive x component

The positive x component of the force acts on Faces 2 and 3: 1 is aligned with the x-axis, and the component is only tangential, while 4 and 5 are directed in such a way that the coupling surfaces pull apart under a force $\vec{F_x^+} = 1\hat{i}$. The $cos(\pi/8)$ term is calculated on the basis that the constant-height arcs are always centred on the middle of the $\pi/4$ arcs, so the chords traced are always at an angle of $\pi/8$ with respect to the closest vertical plane. The forces acting on Face 2 are:

$$F_n = F_x cos(\pi/8) sin(\alpha) \tag{4.12}$$
$$F_t = \sqrt{(F_x sin(\pi/8)^2 + (F_x cos(\pi/8) cos(\alpha))^2} \tag{4.13}$$

The triangular faces at half-quadrant instead are always at a $\pi/4$ angle with any vertical plane, and so the projection comes from the factor $sin(\pi/4) = cos(\pi/4) = \sqrt{2}/2$.
The forces acting on Face 3 are:

$$F_n = F_x cos(\pi/4) sin(\pi/8) \tag{4.14}$$

$$F_t = \sqrt{(F_x sin(\pi/4))^2 + (F_x cos(\pi/4)\cos(\alpha))^2} \tag{4.15}$$

4.3.2 Negative x component

For the negative x component, the opposite of what said in the positive case is true: Face 1 still only receives an in-plane component, while Faces 2 and 3 pull apart from each other. That leaves Faces 4 and 5 to support the force.
For Face 4 the following forces are found:

$$F_n = F_x sin(\pi/8) sin(\alpha) \tag{4.16}$$

$$F_t = \sqrt{(F_x cos(\pi/8))^2 + (F_x sin(\pi/8) cos(\alpha))^2} \tag{4.17}$$

Opposite to what said for surface 1, the x component only has a normal component on Face 5, which is perpendicular to plane xz.

$$F_n = F_x sin(\alpha) \tag{4.18}$$

$$F_t = F_x cos(\alpha) \tag{4.19}$$

4.3.3 Positive y component

For the positive y component only Faces 1 and 2 are stressed; Faces 3 and 4 are pulled apart and Face 5 only has in-plane force.
Face 1 behaves for the negative y component as Face 5 for the negative x component:

$$F_n = F_y sin(\alpha) \tag{4.20}$$

$$F_t = F_y cos(\alpha) \tag{4.21}$$

For Face 2:

$$F_n = F_y sin(\pi/8) sin(\alpha) \tag{4.22}$$

$$F_t = \sqrt{(F_y cos(\pi/8))^2 + (F_y sin(\pi/8) cos(\alpha))^2} \tag{4.23}$$

4.3.4 Negative y component

For the negative y component, Faces 1 and 2 are pulled apart, while Faces 3 and 4 are pushed together. Face 5 has again only an in-plane force.
The components on Face 3 are found as follows:

$$F_n = F_y sin(\pi/4) sin(\alpha) \tag{4.24}$$

$$F_t = \sqrt{(F_y cos(\pi/4))^2 + (F_y sin(\pi/4) cos(\alpha))^2} \tag{4.25}$$

Finally, the components on Face 4 are:

$$F_n = F_y cos(\pi/8) sin(\alpha) \tag{4.26}$$

$$F_t = \sqrt{(F_y sin(\pi/8))^2 + (F_y cos(\pi/8) cos(\alpha))^2} \tag{4.27}$$

4.4 MATLAB script

In the main script are first defined the boundary conditions of the problem, as well as the width of the steps for the parameter iterations. Then, custom created functions are called, to perform subsequent operations, and to perform the same operations on different geometries.

Equation 4.6 determines which tolerance is stricter between linear and angular, by considering all the given boundary conditions and geometric dimensions. The stricter condition is set as the lower boundary of the interval where the geometric parameter γ is cycled; the upper limit is given by Equation 4.3 where R_{ext} is set as the outer radius of the base-plate. Two vectors are then created: one containing all the values of the parameter in the interval, the other containing the values of the external radius corresponding to each value.
Then, cycling on the geometric parameter, the projections on the plane *xy* and on the planes *yz* and *zx* of all the different surface shapes are calculated. In this step, the areas' projections on the vertical planes of the three-sided surfaces are calculated with an approximation that sees the curved sides as triangles instead. This imprecision makes the area formula less complicated and does not impair the accuracy of the model, and instead, this underestimate contributes to adding a factor of safety of unknown entity.

4.4.1 Cycling through the parameter values

When cycling through the parameter values, the operations are made as if the coupling surface was divided into quadrants, and the coefficients by which the forces are multiplied on each face are obtained by combining the area projection fraction of said face and its orientation.

First, the coefficients matrix is created, which determines the behaviour of each face in one quadrant against the x and y components of a force on the *xy* plane; an array with the equations to use for each face is created: Equations 4.9 and 4.11 are combined to obtain the value of P. It becomes evident from the following equation that using P as data and F as an unknown would have required a numerical solution instead of the direct solution found. This is what is obtained after combining them and isolating P:

$$P = \frac{F_t - \mu F_n}{sin(\alpha) + \mu cos(\alpha)} \tag{4.28}$$

Cycling through four quadrants, and through the five faces in every quadrant, a check on the discordance between face normal and component direction is performed, to perform the calculations only where necessary, leaving zero all the other components of the results vector.
For every parameter value, the maximum of the results vector is taken as the value of the failure force, as said beforehand: the failure of the static friction on one face brings to a cascading failure on all faces.

The results in the next section show calculations made for three values of the coefficient of static friction of the material, to highlight the difference it makes on the phenomenon. The values are taken in an interval around the chosen value, with caution not to exit the boundaries found in [14]: the three values of μ used are 1.05, 1.2 and 1.35.

4.5 Results

The load applied to obtain the results is aligned with the x-axis, and its entity is 600 N: the value is selected according to what said in Section 2.1, with a factor of safety of 1.5 over the maximum weight of the module. The alignment with an axis of the plane is the most critical load condition because of how the projections of the areas are distributed, which spreads the force on a larger area.
The requested data from the script are the required pre-tensions of the interface locking mechanism to hold in place the two coupling surfaces employing static friction in case of a 600 N tangential load (this value comes from the load given by the block's maximum weight (400 N) multiplied by a factor of safety of 1.5).

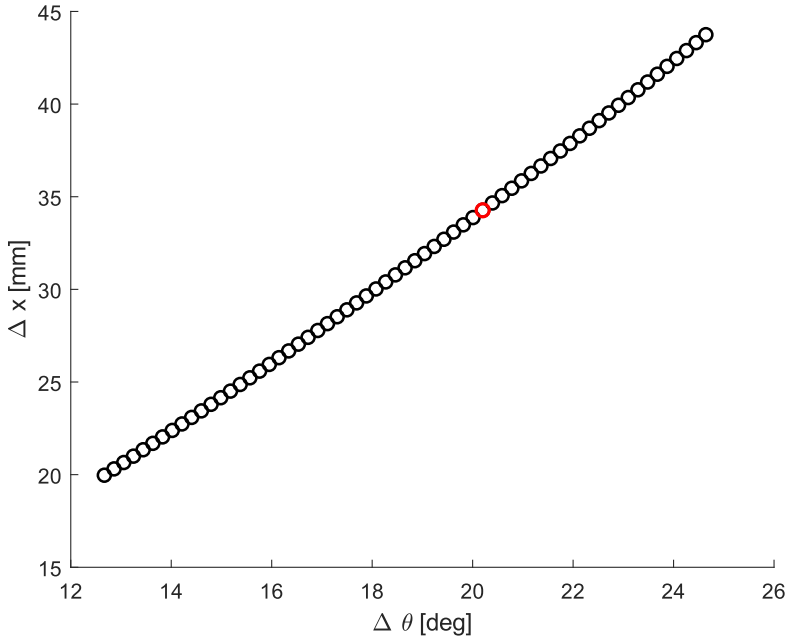

Figure 4.2: Relation between angular tolerance δθ and linear tolerance δx.

In Appendix B is a table of geometric dimensions that come from the mathematical relations of Section 4.1, plus the final results of the script that applies the mechanical laws to find the normal force of failure for the static friction.
The dimensions selected to be listed are $[\gamma,\ R_{ext},\ \delta,\ \delta x,\ P_{min}]$: the first is the variable through which the geometry is changed, δ *and* R_{ext} are the dependent variables that change with γ, and δx is the linear coupling tolerance, while γ itself is the angular coupling tolerance, P_{min} is the final result requested to the script.

Figure 4.2 highlights the significant improvement in the tolerances required from the assembling apparatus: the linear tolerance δx goes from 5 millimetres without the coupling surface to 3.4 centimetres in the case selected (highlighted in red in the graph), and the angular tolerance $\delta\theta$ is broadened to twenty degrees.

The alignment of the force with an axis of the plane is the most critical load condition: if the same load was divided equally between x and y components (direction of the lateral force coincides with the bisector of the first quadrant), the results show that the force required by the locking mechanism is lesser than that at the corresponding point in the table, at the boldened row—which highlights the parameter value chosen for the geometry of the component. The force required from the locking mechanism in case of lateral load applied along the 45° line is $F_{45deg} = 2794.39N$.

The load case analysed takes the hypothesis of an operation performed on Earth (the reason for using $g = 9.8m/s^2$ as acceleration to convert the weight into a force); the actual value of Aluminium on Aluminium friction coefficient is $\mu \approx 1.1$, used in a different run of the script, which

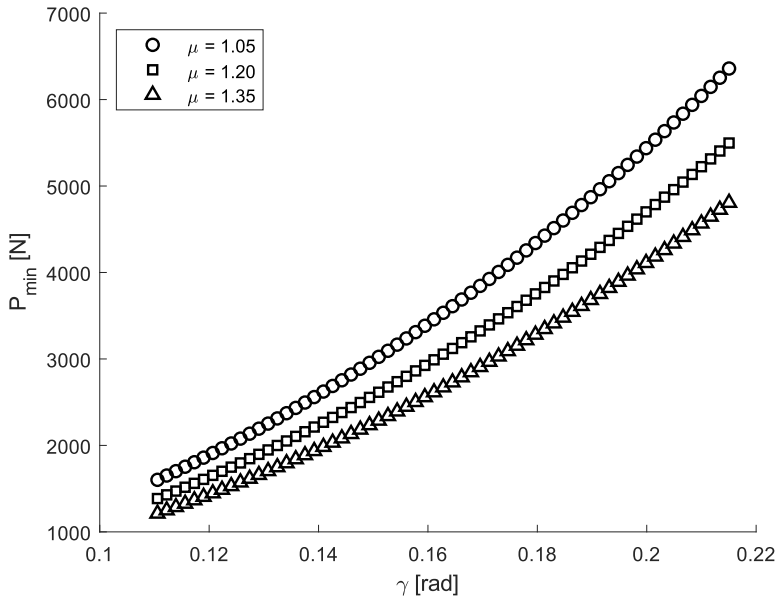

(a) The value of the parameter γ goes from about 0.11 rad (6°) to 0.22 rad (12°).

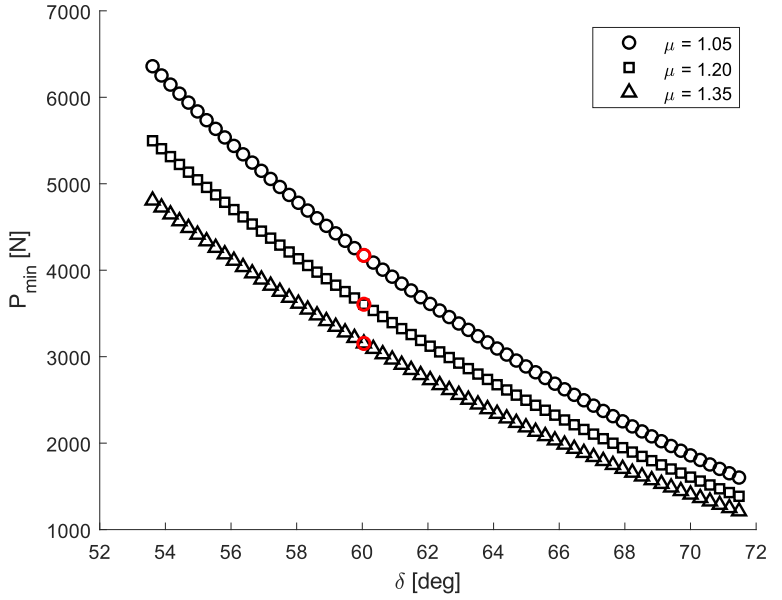

(b) The value of the parameter δ goes from about 50° to 70°.

Figure 4.3: Plots of P_{max} over both γ and δ. $\mu = [1.05,\ 1.2,\ 1.35]$ defines the three different curves.

results are shown in Figure 4.3. The value of the force required from the locking mechanism at the chosen geometry parameter is 2422.37 N, and it does not exceed its failure stress. Therefore, the locking mechanism can provide the normal force to prevent the coupling surfaces from sliding on one another, without incurring in critical failure.

To explain more in detail the results are shown in Figure 4.3: To better show the behaviour of this datum at the change of the parameter, a curve is plotted, with the parameter γ on the x axis, and the pre-tension required on the y axis; moreover, the maximum radius allowed is increased to increase the field of view of the graph.

As one can see, the required force increases when the angle γ increases, because the height of the coupling surface is fixed at h_{tot} =60 mm, which corresponds to two times the thickness of the iBLOCK walls. This way the coupling surface does not pass through the inner side of the wall, and so it does not invade the internal volume of the iBLOCK; however, this solution flattens the coupling surface when the γ angle increases, causing the load to be more and more tangential to the inclined surfaces. The projection on the plane of the inclined surfaces is the component that has to be balanced by the static friction force, and because the former increases, the latter has to increase as well.
To make it more explicit, in picture 4.3b is plotted the behaviour of the pre-tension with the change of δ, which is the angle the inclined surfaces have with the vertical to the *xy*plane. As predicted, an increase of δ leads to a decrease in the pre-tension required by the locking mechanism, for the inclined surfaces become increasingly vertical.
In the graph in picture 4.3b the circles show the value of δ used to build the geometry analysed in a Finite Elements Model.

4.6 Static friction failure

Failing to reach this condition would not mean an automatic failure of the coupling surface in its role to hold the interfaces together, but its failure of doing so through static friction. The system is still held in position thanks to the locking mechanism of the iSSI, and the lateral loads on the coupling surface's inclined faces are replaced by a moment: the lateral force is not applied on the interface plane, but rather on the centre of mass of the block it holds, which is, for the sake of simplicity, in the geometric centre of the cube. This creates a moment at the interface, and here are the mathematical equations to find out the required force from the locking mechanism to equilibrate the weight:

$$M_W = F\ p = P_{max}\ L/2 \tag{4.29}$$

$$M_R = -R\ p_r = -R\ r_{coupling} \tag{4.30}$$

The centre of rotation is the lowest point of contact between the two coupling surfaces because it is the point that suffers the most the compression forces, while the upper halves of the coupling surfaces will get pulled apart. Therefore, looking at Figure 4.4, from the equilibrium of moments, follows:

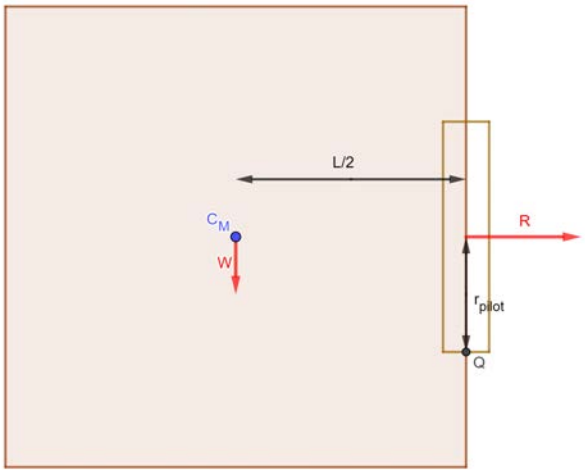

Figure 4.4: Schematic representation of a module—for the sake of our model, it is fixed in Q with a hinge.

$$R = \frac{L/2}{r_{coupling}} P_{max} \approx 2P_{max} \tag{4.31}$$

The coupling surface diameter is about half the size of the module; because the moment radius for the constraint reaction is half the moment radius for the weight, the constraint reaction must be double the entity of the weight to balance it out. Therefore the load on the locking mechanism when the module is hanging sideways is twice the load the same module consists when hanging vertically.

One possible improvement to the design would be making so that the modules had a contact point at the sides' edges: this would decrease the constraint reaction radius to equal the weight radius, ensuring that the same load that is supported normally is supported tangentially as well.

4.7 Validation

The MATLAB code written is however in need of some sort of validation, if the results are to be considered of any significance.
The actions that had to be translated to MATLAB code were essentially two: calculating the area of the faces' projections on the vertical planes and applying the balance of forces to the mechanical laws. These are the points that have to be proved, for the results to be accepted as valid.

As proof of the above point: increasing the coefficient of friction to a very high value should give a minimal value of pre-tension required. This is already proved by the increase in the force required to hold the two surfaces in place, at the lowering of the static friction coefficient.

For the latter: a value of the parameter is picked, and the results of the area fraction from the script are compared to the values obtained by manual calculation. The results are obtained comparing the areas calculated by the script for the chosen parameter to the areas of the projected surfaces in the CAD model built.
The information given by the comparison is the following:

- The projected areas, ordered by magnitude, take the same order both as calculated in the script and obtained by projection
- The largest (relative) error obtained is of 13%, considering the true value the area obtained from the CAD model.
- The relative error is largest for the trapezoidal faces, and it brings to an overestimate of said areas

5 Finite Element Simulation

The first task to fulfil through the finite element simulation is to prove the coupling surface does not encounter structural failure while carrying out its function; the second task is to provide feedback data on the possible modifications to the structure.

MSC Patran™ Student Edition is the Finite Element model creator used in this work. It allows the user to start a model from scratch or to import the geometry from different formats (e.g. Parasolid, the format used in this work). After the creation of the component geometry, all other elements must be created and associated with it: constraints, loads, properties and mesh. The software allows to apply properties directly to the geometry items; it then automatically applies them to the nodes when generating the job.

5.1 Assumptions and boundary conditions

The piece is modelled as a metal sheet, because of the nature of the component and its form factor. The use of 2D QUAD elements—instead of 3D HEXA—aids the accuracy of the model because the form factor of the piece (metal sheet) would cause high element badness in a 3D model, and possibly lead to elements Shear Locking, the phenomenon in FEA where linear elements do not portray well enough the bending condition, causing shear stresses (and consequently shear deformation) to appear.
The edges are modelled with sharp angles instead of blends between faces: the precise radius obtained in the piece manufacturing is unknown, and during the process of building the mesh, the elements obtained on arbitrary blends were highly irregular—an issue that causes numerical errors in the simulation. Moreover, a blended edge distributes internal stresses, reducing stress concentration: having sharp edges in the FE model serves as an additional factor of safety over the real phenomenon because this way the stress distribution, in reality, is lower than the stress distribution obtained in the model.

The load case to analyse is two coupling surfaces that push into each other with a determined force; in the model one surface is represented and to it are applied forces distributed solely on the walls that push against the hypothetical other surfaces. This approach avoids complications arising from modelling contact between two pieces and allows a precise meshing of the piece while remaining within the limit to the number of elements fixed by the MSC Nastran™ Student Edition.

5.2 FE Model

5.2.1 Geometry

The first step of building the model is to extract the coupling surface from a solid piece in the CAD software: just the upward-facing surfaces are selected and kept for the FE simulation. Once the surfaces are selected, they are exported to a Parasolid file; this allows to import it to MSC Patran™, which creates 16 distinct surfaces not linked to each other, as shown in picture 5.1. Note that Parasolid is not the only format available to import a file from Siemens NX™ to Patran™, but both support it, and it is the default format to which both software directed.
One step to take particular care of is to force the software to import the piece in the chosen unit of measure; otherwise, the results might be challenging to interpret, requiring to perform manual conversions to go back to SI units.

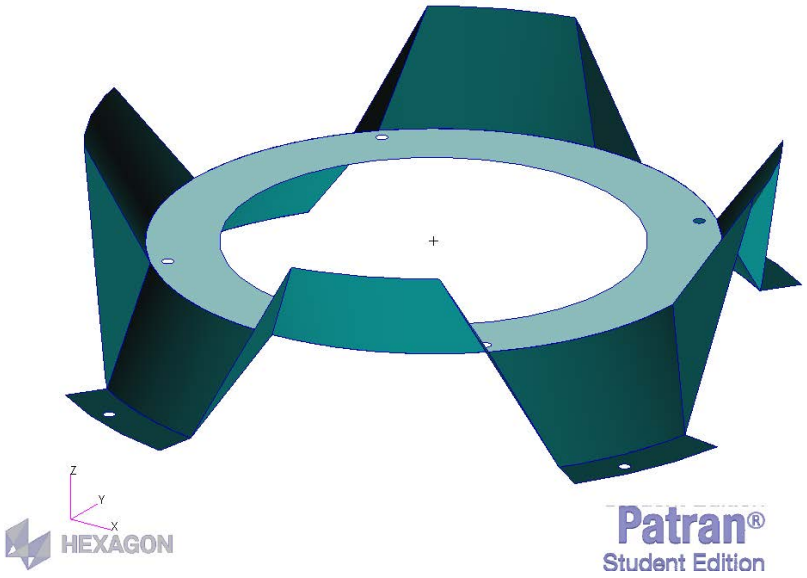

Figure 5.1: The outline of the surfaces created by MSC Patran™ after being imported.

From these geometry elements, new points have to be created at the centres of the fastener holes, that will be used to fix the structure to the ground.

5.2.2 Properties

MSC Patran does not have an integrated material library, so the material properties must be manually inserted: the isotropic material Al7075 is created, and to it are assigned the values: E = 71 GPa, γ =0.3, $\rho = 2810[kg/m^3]$.

A new shell property is then created with thickness t = 3 mm and material *Al7075*, and it is assigned to the surfaces of the geometry.

In the Nastran .bdf file, the previously described operations create the fields:

- MAT: defines the Material field, and gives it a reference ID and its properties;
- PSHELL: defines the Shell property, assigning it a reference ID, a material (identified by its ID) and a thickness.

5.2.3 Loads and boundary conditions

The load analysed in the model is the worst-case scenario and, as seen in section 4.5, that is for a given force to be oriented with one axis of the plane. Because this force is supposed to be applied to the centre of mass of the module, a point is created at its position, to which the force is then applied. The point lays on the axis of the coupling surface, at a distance of 20 cm from the interface plane, at coordinates [0, 0, 200] mm.

As for the constraints applied to the model, the mounting points have to be fixed to the ground: because those points are holes where bolts have to be inserted, the border of the hole in the zone of the model that must be fixed. This operation has to be done using a spider-like formation, where a node in the centre of the hole is fixed to the ground, while the rotational degrees of freedom are left untouched. Multi-Point Constraints are created between the centre point and the hole's edges, with RBE2 (Rigid Body Element) selected as the Multi-Point Constraint type. This type of element creates a rigid connection between nodes, where the displacements at one or more nodes are dependent on the displacement of the independent one[16].

5.2.4 Mesh and Multi-Point constraints

Typically, to generate the mesh, one would first create the mesh seed on the edges of the surfaces, then mesh the surfaces: this allows more freedom in the form the mesh takes and more accuracy in the creation of elements.
Unfortunately, this course of action is not available because of some property of the imported geometry that prevents the creation of a mesh seed on the curves. The approach used instead is to mesh directly the surfaces, using Patran's Paver feature, setting the element dimension to determine the number of points in each edge. This approach causes the mesh to be more irregular than if the process could be controlled better, but the results are still acceptable.
A node is then created on the point to which the force is applied.

After the mesh is created on all the surfaces, a nodes equivalence is performed, to delete and merge nodes that are closer than a given distance, which is set to 0.01 the dimension of the model.

Once the mesh is assigned to the piece, it is time for the Multi-Point Constraints to be built, between the force application point and the surfaces where the force is applied. The type of MPC chosen for this task is RBE3. This type of Multi-Point Constraint transfers forces between the independent and dependent nodes, defining the displacement at a reference node equal to the weighted average of the displacements of a set of other nodes[16].

In the .bdf Nastran input file, these operations correspond to the creation of a set of CQUAD and CTRIA entries, each one assigned the PSHELL property earlier defined, and each one corresponding to one plane element of the FE model. An RBE3 field shows the nodes connected by this multi-point constraint.

5.2.5 Launching the job

After the model is complete, the job can be created as a .bdf file and then invoked from MSC Nastran. The job is created with care to un-check the box "Automatic Constraints" in the Solution Parameters: this makes so that the degrees of freedom fixed in the model are exclusively the ones selected by the user, and Nastran does not add ulterior constraints that help the job run in case of matrix pivot ratio errors (free bodies in the model), but at the same time prevents the user from verifying whether the model is set correctly, and sometimes generate wrong results. No further changes are made to the default settings before generating the .bdf Nastran Input file.

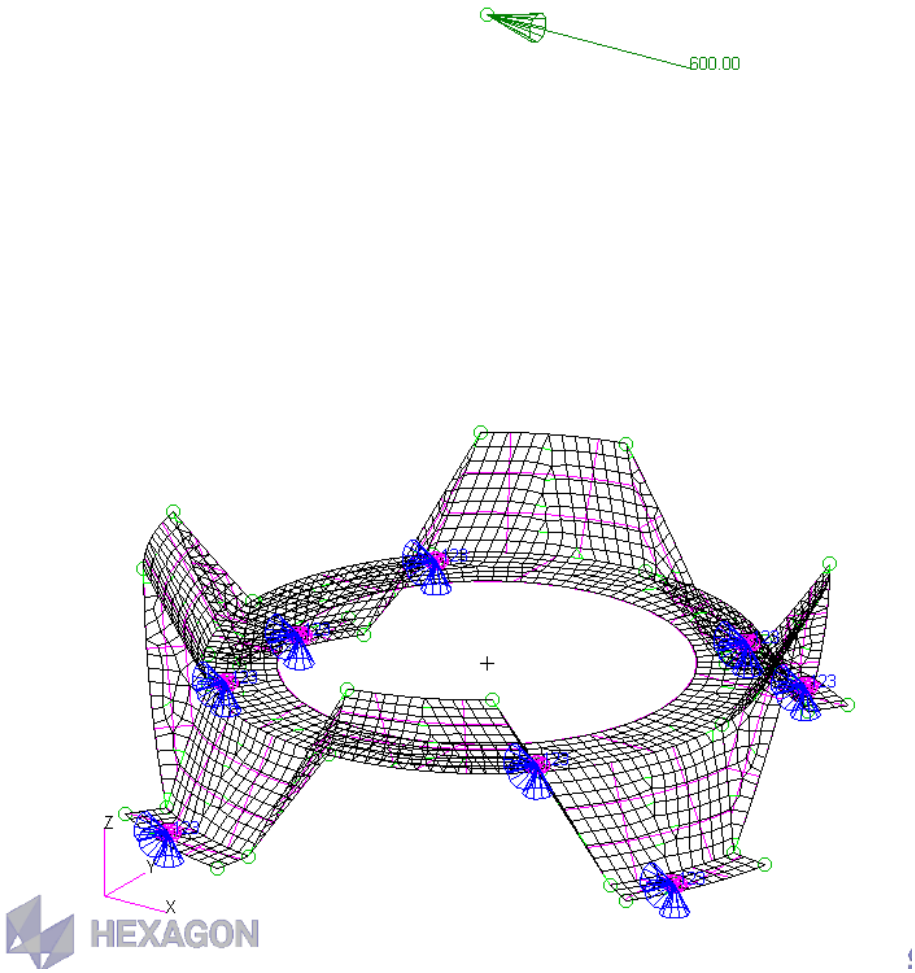

(a) The representation of the boundary conditions (fixed nodes) and the load applied to the model.

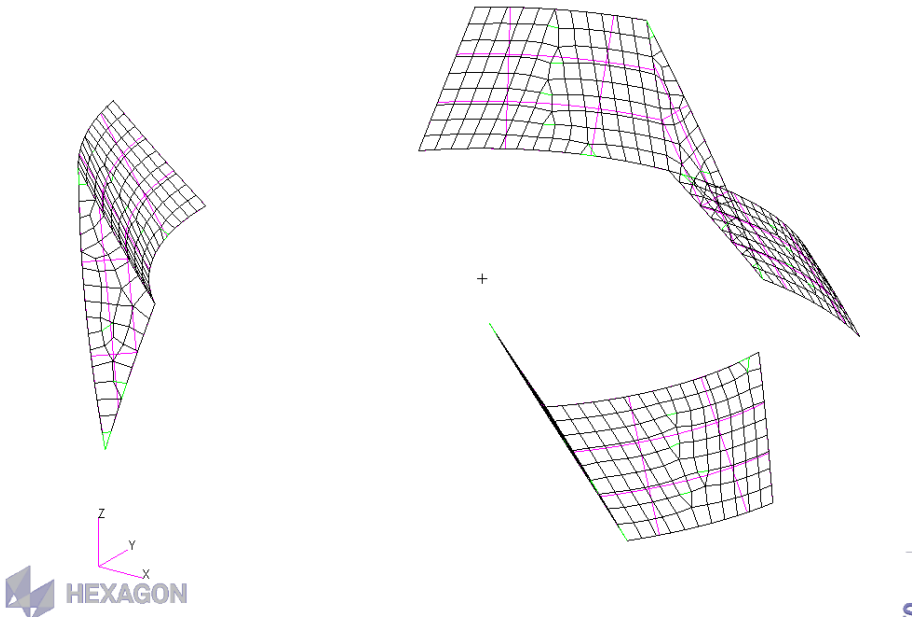

(b) The surfaces that support the lateral load in direction $\hat{F} = -\hat{\imath}$.

Figure 5.2: FE model in its entirety and selection of loaded surfaces.

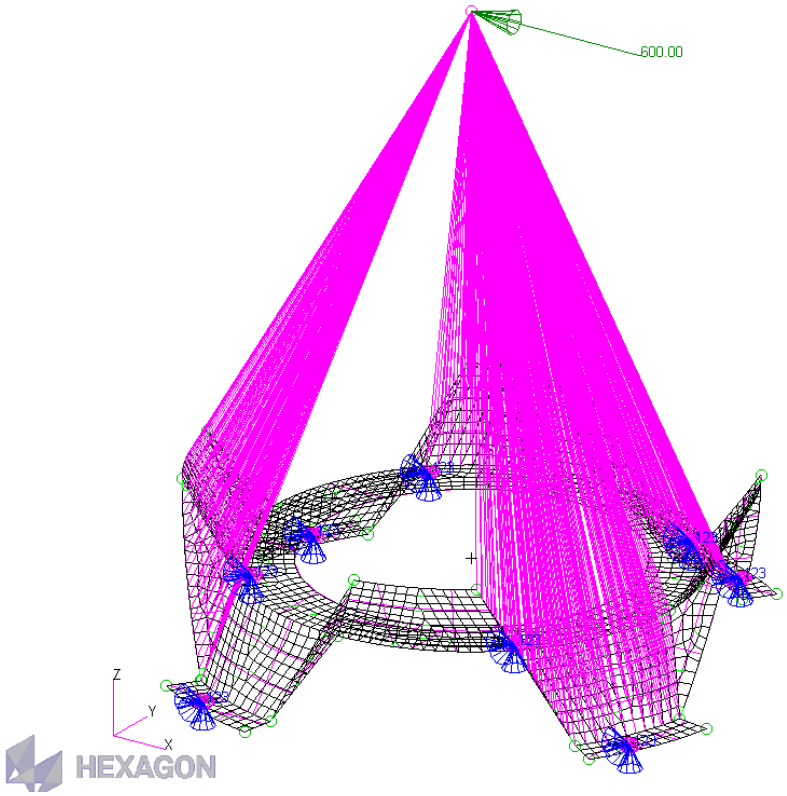

(a) The representation of the meshed surfaces plus the Multi-Point Constraints that link the stressed faces to the Point of Application.

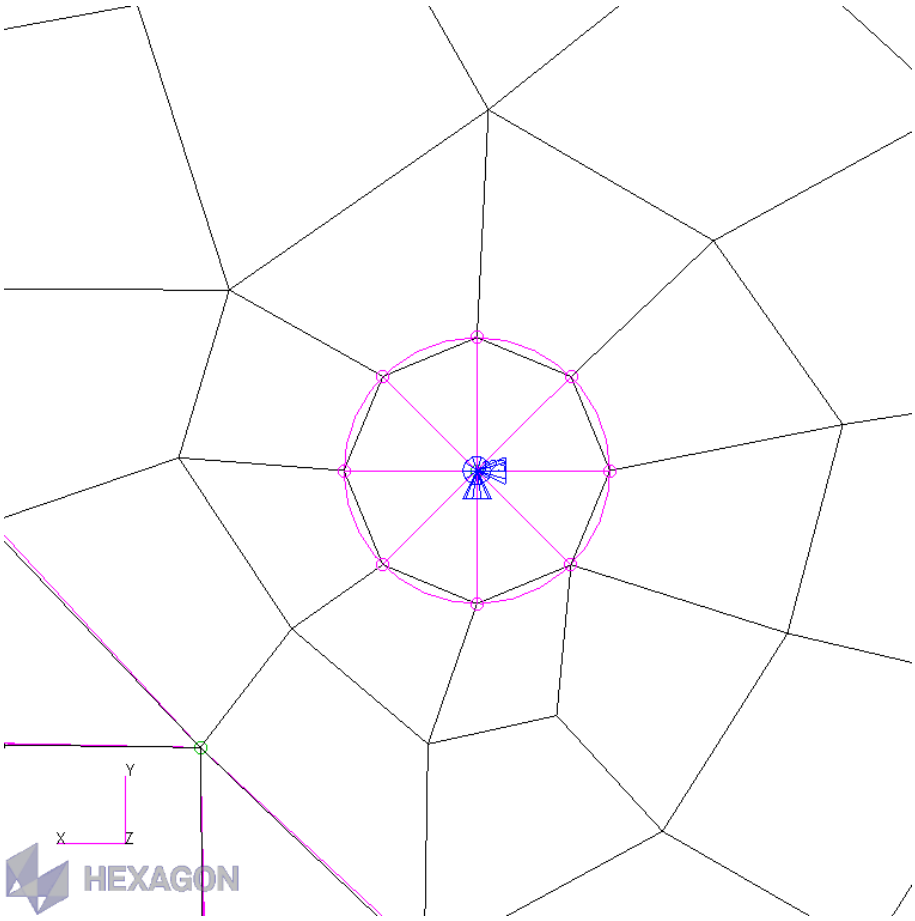

(b) Enhanced detail on the Multi-Point Constraints that link the bolt to the hole edges.

Figure 5.3: Details of the model.

5.3 Results and discussion

After some post-processing, the results obtained are shown in Figure 5.4. The maximum stress (full-scale value) in the material is *190 MPa*, less than half the value of the material yield stress (see Section 2.4). This guarantees that the material, modelled under the previously described assumptions, does not fail when subject to the force applied. There is, moreover, a factor of safety of 2.37 on the load condition.
The maximum displacement is found in the tip of one of the protruding ledges, and its value is of about *0.6 mm*, which is about one-fifth of the thickness of the sheet.

5.3.1 Interface normal load

Because the component connects both to the frame and the interface, the load the interface supports in the normal direction must travel through the interface to reach the frame. It should be further noted that the bolt holes on the support ring flanges have corresponding holes on the base-plate: these imply that bolts can be conducted through both of them to transfer loads directly to the frame instead of passing through the coupling surface; the test was carried out regardless, to check whether the designed component could withstand said loads.
The load considered is in this case, as shown in figure 5.5a, the same force applied in the case already studied, but directed normally to the plane of the interface; the constraints are this time bolts applied only to the outer support flanges, while the inner mounting points are those to which the load is applied.

As can be seen in figure 5.5b, the maximum stress inside the material is in the order of 200 MPa, which is widely lower than the yield stress for AL7075. The component is, therefore, able to withstand this load case with a large margin.

Mass optimization can be performed on the component. This would require to slightly modify the design to accomodate the design of the interface itself and the position of mounting points, while maintaining a condition of perfect matching when the middle-surfaces are touching. A design similar to that of NASA Docking System could be considered, in order to further decrease the component's mass, although taking into account the decrease of mechanical performances that accompany such choice.

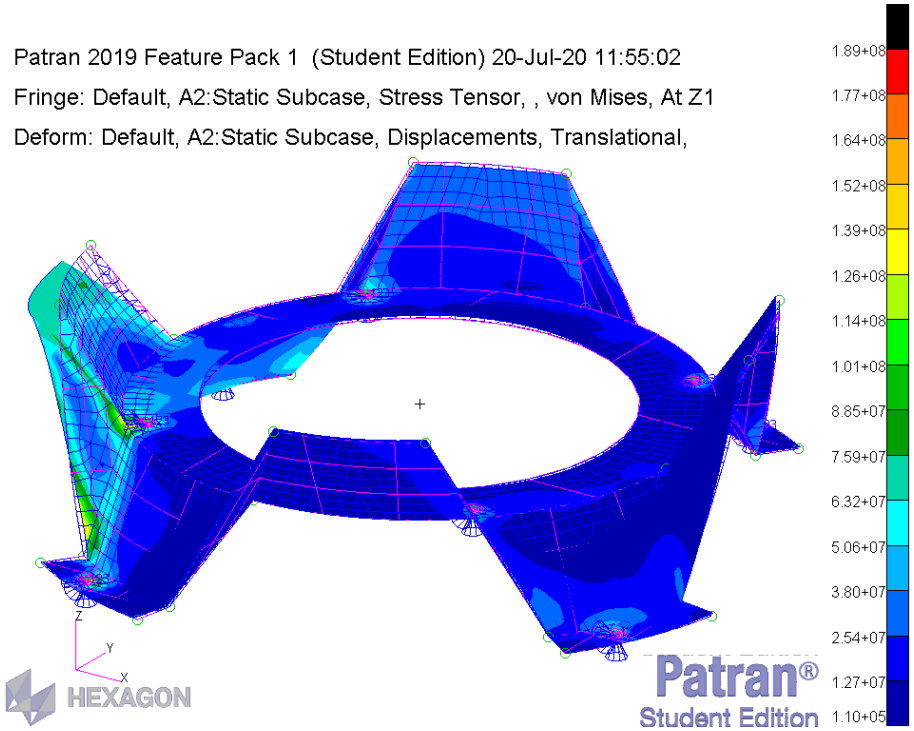

(a) Deformation and color-graded scale of the internal Von-Mises stresses results.

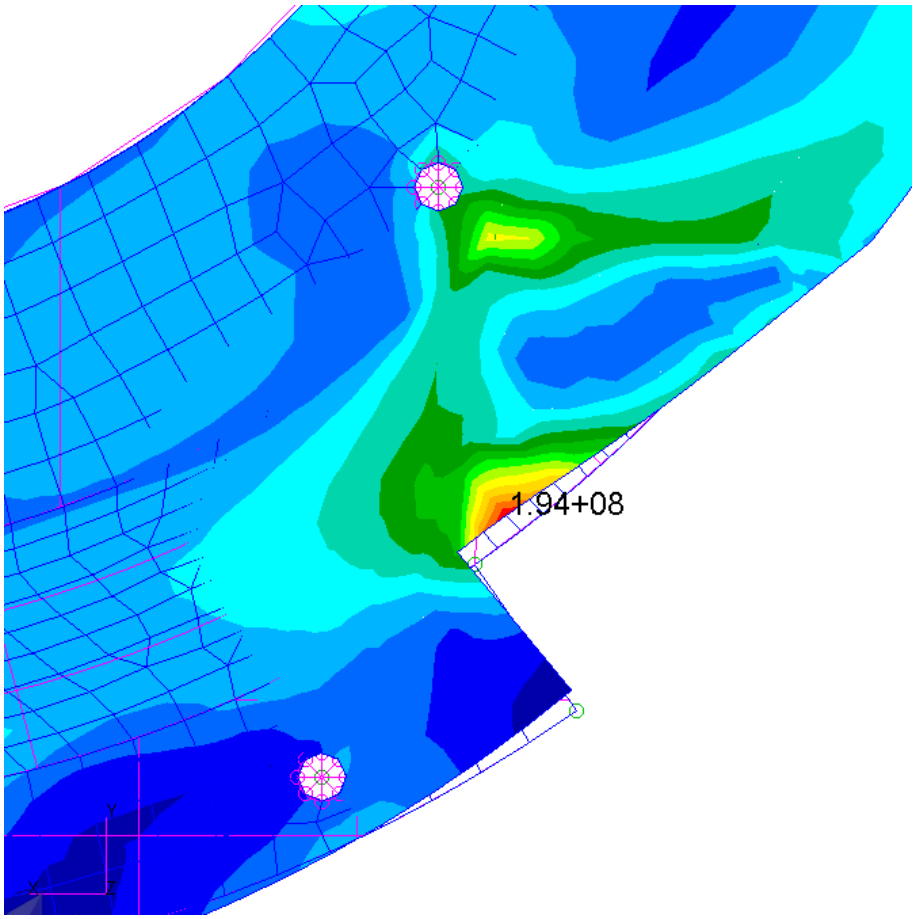

(b) Enhanced detail on the most stressed point of the coupling surface, on the edge of one of the slopes.

Figure 5.4: Results of the FE analysis conducted on the component.

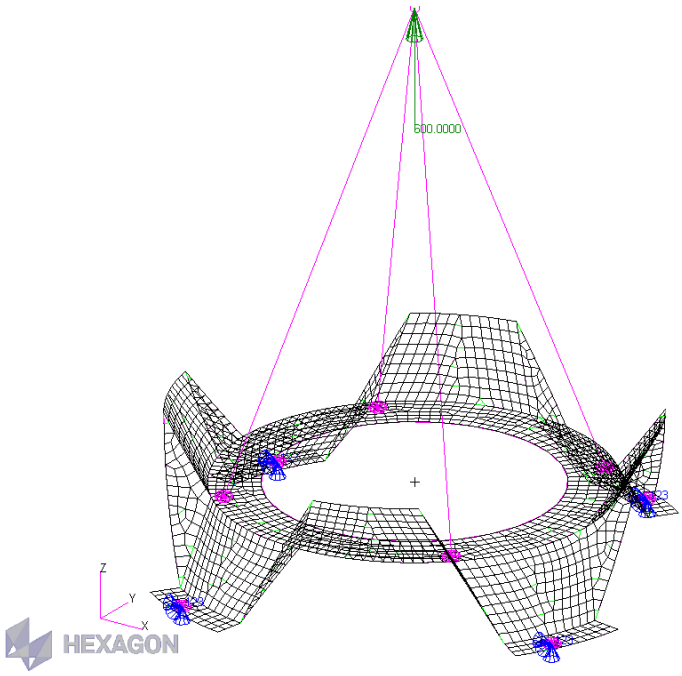

(a) Model, boundary conditions and load.

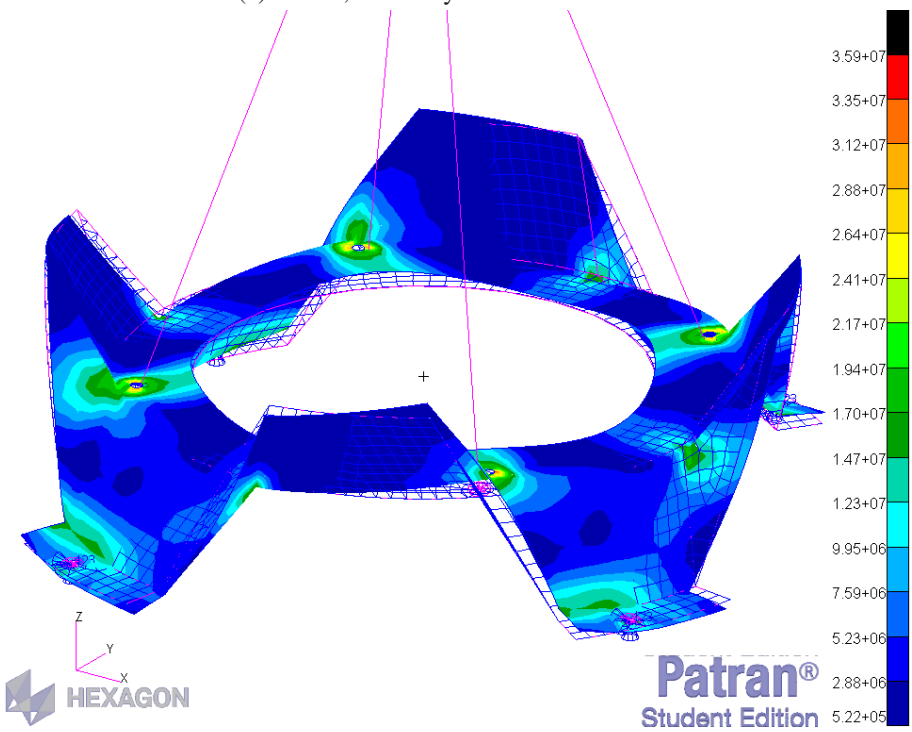

(b) Results.

Figure 5.5: Load case and results of normally loaded component.

5.3.2 Model inaccuracy

It is necessary to point out the possible ways the model created is not an accurate representation of reality:

- Modelling only one of the two surfaces interacting is a choice partially forced by the limit to the number of elements given by MSC Nastran™, but it means removing constraints to the surfaces, which would push against each other while deforming.

- The sharp edges of the inner bends lead to stress concentration, which could lead to an inaccurate representation of the stresses.

- The position of the maximum stress point on one of the outer edges is worsened by the fact that the material is stretched in that point, because of the manufacturing method. This may lead to higher stress on that point.

Regardless of these inaccuracies, the model is adequately representative of the load condition to which the surface is subject.

5.3.3 Verification

The model, as the MATLAB script did, needs verification. The method to verify the validity of the FE model is to apply to its boundary conditions with notable results, and compare said results to those of the simulation. Because a Linear static solution is the most straightforward possible simulation, two proofs will suffice: a simulation is set with a load value of 0, which should result in an utterly inert structure; a second proof is to perform a Normal modes research, which will provide a 0 Hz eigenfrequency if there are free bodies.

Both verifications are confirmed by the model, which can be therefore assumed as valid.

5.4 Mounting points

The maximum stress is not on the edge of one of the mounting points: this is somehow comforting because usually, these are the first failure points of structures. The stress magnitude allows the material to carry the stress without failure; nevertheless, the issue has to be placed on whether the fasteners can withstand the stress that results from the load condition.

Because the constraint in the FEA result is localised on one node, the total Constraint Force is immediately available from the results file, even if the post-processing images do not show it: the maximum SPC (Single-Point Constraint) force generated is *[934.0, 386.7, 391.4] N*.
This results in a *1084 N* maximum force supported by one bolt. It has to be divided by the area where the force is applied, which is:

$$\begin{aligned} A &= d * t \\ &= 3mm * 3mm \\ &= 9mm^2 \end{aligned}$$

The shear stress acting on the bolt is therefore:

$$\begin{aligned} \tau &= 1084[N]/9[mm^2] \\ &= 120.444[MPa] \end{aligned}$$

This value is widely lower than the strength of steel, the material of the bolt: this ensures that no bolt enters a failure state.

6 Conclusions

6.1 Results

The result of the work is a design for a coupling surface that satisfies all the primary requirements asked from it: it broadens the tolerances required for the alignment of two interfaces, and in the connecting position, the interfaces are aligned within the tolerances required for coupling. The component can also be mounted to the interface through already present bolt holes, without any need to modify the interface's already established design.

The chosen geometry does not conflict with the pre-existing pieces, thanks to the choice of a metal sheet form factor.
The manufacturing of the component, by bending or deep drawing a metal sheet, and the use of Aluminium alloy Al-7075 allow a lightweight component and an adequate level of manufacturing scalability.

The piece also carries out the secondary function of lateral load transfer: the coupling surface is able to withstand loads to which the interface has been previously tested, and the static friction between the faces is enough to support the loads without the connected module becoming a suspended shelf. The thickness, which value is chosen by the boundaries provided by the interface's already estabilished design, allows the material to carry the stresses while staying widely within the elastic regime.

6.2 Discussion

The work has possibly overlooked some points that should be taken into consideration for the completion of the design and the product manufacturing, mostly for lack of knowledge on the part of the author. This is the place where those omissions are discussed and motivated.

The piece tolerances that come from the chosen manufacturing method are unknown, because of limited knowledge regarding deep drawing, and more generally of manufacturing methods. Moreover, as was already said, the slopes are at risk of resulting thinner than the designed thickness because of the stretching the metal needs to go through to develop. For these reasons, the possibility of manufacturing the piece by die-casting or machining should not be tossed aside, until these critical points are cleared.

The hard vacuum found in space can bring out peculiar behaviour from materials: one of these is cold welding between surfaces in contact, because of the absence of a process of re-oxidation of surfaces after the coating (natural oxide layer, chemical film or metal coating) is removed because of impact or fretting[17]. Satellite lives are very long, for the intrinsic nature and cost of space missions: this could cause cold welding between the two metal surfaces that must stay in close contact for the entire duration of the mission, and possibly complicate the operations of module release in case of orbit service/maintenance.

Finally, possible future developments of the coupling surface could study the feasibility of a multi-purpose coupling surface that also carries out the function of the thermal interface. This problem could require particular surface treatments that change the characteristics of contact and friction between two coupling surfaces, and would definitely require a heat conduction system between surface and payload to be designed (from scratch, or with the Thermal interface component of iSSI as a blueprint).
One such surface modifier could be the coating of the surface using carbon nanotubes, directed perpendicular to the surface itself, so that the heat may be carried along their length. This allows, thanks to CNT's very high thermal conductivity, to maximize the heat exchange between the surfaces.

6.3 Final considerations

The possibility to have serviceable satellites is a feat that would vastly improve the quality of space services in terms of upgradeability, and ultimately an approach with a better understanding of the future's needs. It is now common knowledge that the space environment is in fact becoming more and more crowded, not to say littered: being able to not increase the number of orbiting objects to upgrade a satellite's service or restore a non functioning satellite is a step towards what will one day become the operation of de-orbiting space pollution—or at least the most dangerous pieces—and to not worry excessively about the damage that the remaining pollution could do to operative satellites' systems.

Additionally, the iSSI interface is a technology that may be applied on different fields on earth as well, from multi-functional appliances to transportation [18] to, potentially, modular housing units, made of multiple so-called "tiny houses".

Bibliography

[1] Cooperation PROJECT. 'Final Technical Report of the Cooperation Project iBOSS - Intelligent Building Block Concept for On-Orbit-Satellite Servicing and Assembly'. Oct. 2018.

[2] Martin KORTMANN et al. Building Block-Based "iBOSS" Approach: Fully Modular Systems with Standard Interface to Enhance Future Satellites. en. Tech. rep. RWTH-2016-04239. Conference Name: 66rd International Astronautical Congress. Lehrstuhl und Institut für Strukturmechanik und Leichtbau, 2015. URL: https://publications.rwth-aachen.de/record/658459 (visited on 05/08/2020).

[3] iBOSS Website (old). URL: https://www.iboss.space/.

[4] Martin KORTMANN et al. 'Design and Qualification of a Multifunctional Interface for Modular Satellite Systems'. In: Oct. 2018.

[5] WENZEL. 14th Symposium on Advanced Space Technologies in Robotics and Automation (ASTRA 2017). URL: https://robotics.estec.esa.int/ASTRA/Astra2017/Presentations/21%20June%20Wednesday/5B%20Orbital%20Robotics/S.B5_15.15_Wenzel_Presentation.pdf.

[6] Justin MCFATTER, Karl KEISER and Timothy RUPP. NASA Docking System Block 1: NASA's New Direct Electric Docking System Supporting ISS and Future Human Space Exploration. en. In: (May 2018), p. 14.

[7] International Docking Standard - gallery. URL: https://internationaldockingstandard.com/gallery.html.

[8] SENER SIROM OFFICIAL WEBPAGE. URL: https://www.aeroespacial.sener/en/products/standard-interface-for-robotic-manipulation-sirom.

[9] SENER SIROM OFFICIAL DATASHEET. URL: https://www.aeroespacial.sener/en/pdf-profile-project/standard-interface-for-robotic-manipulation-sirom.

[10] Space Applications Hotdock Official Webpage. URL: https://www.spaceapplications.com/products/hotdock.

[11] Thomas Andreas SCHERVAN et al. Design Strategy, Numerical Analysis and Testing of a Modular Satellite Structure. en. Tech. rep. RWTH-2018-00687. Conference Name: 68th International Astronautical Congress. International Astronautical Federation (IAF), 2017. URL: https://publications.rwth-aachen.de/record/712742 (visited on 05/08/2020).

[12] Whittick MURACA. Materials data handbook: Aluminum alloy 7075. Tech. rep. NASA, Apr. 1972.

[13] D H BUCKLEY. Friction characteristics of single crystal and polycrystalline aluminum oxide in contact in vacuum. en. In: (Sept. 1966), p. 16.

[14] Dudley D. FULLER. Coefficient of Friction. Tech. rep. University of Columbia, Dec. 1968. URL: https://web.mit.edu/8.13/8.13c/references-fall/aip/aip-handbook-section2d.pdf.

[15] Martin KORTMANN et al. 'Multifunctional Interface for Modular Satellite Systems with Robotic Servicing Capabilities'. In: Sept. 2017.

[16] MSC SimCompanion - MSC Nastran 2019 Quick Reference Guide. URL: https://simcompanion.mscsoftware.com/infocenter/index?page=content&id=DOC11931 (visited on 11/08/2020).

[17] STM-279 Assessment of the Cold Welding between Separable Contact due to Impact and Fretting under Vacuum. en. Nov. 2009. URL: https://www.esa.int/About_Us/ESA_Publications/STM-279_Assessment_of_the_Cold_Welding_between_Separable_Contact_due_to_Impact_and_Fretting_under_Vacuum (visited on 11/08/2020).

[18] UpBus - Short range modular transportation. URL: https://www.upbus.rwth-aachen.de/index.php/home-en.

Appendices

A MATLAB code

A.1 Main script

```
% Param.m is the main script: it calls for the functions created to
    perform certain tasks and it performs certain tasks itself to
    convert output of certain functions to the input of others

% Calling some commands to clear the screen and objects opened in
    scripts run previously

clear all
close all
clf
clc

%% Introduction of constants of the problem
R_i = 80.5;         %[mm] Outer radius of the iSSI
H_tot = 59.7;           %[mm] 2x height of the iSSI
F_in = [600, 0, 0];  %[N] Object weight = about 40kg, FoS = 1.5
% F_in = [480, 0, 0];  %[N] Object weight = about 40kg, FoS = 1.2
% this [N,0, 0] is max strain on the static friction because the
    weight is not distributed between the two planes
% P = 400;          %[N] Pre-tension given by the iSSI

%Tolerances to be reached with the robotic arm:
gamma_tol = 2*pi/180; %[deg] angular tolerance
dx_tol = 10;          %[mm] linear tolerance

%An arbitrary ceiling to the value of R_e: 10cm of added radius
R_e_max = 102.5;
% R_e_max = 200;

%% We build the geometry and compute the projections of surfaces on
    the three main planes.

% [gamma, R_e] = geometry(R_i, dx_tol, gamma_tol, R_e_max, H_tot);
% The function is not used, the  operations are carried out in the
    main script instead

% Strictest condition on gamma_min is taken as gamma_min
gamma_min = 2 * asin( 1 / (2*(1+R_i/dx_tol)) );
gamma_min = max([gamma_tol,gamma_min]);
```

```
%Maximum value of gamma, assumed the limit on R_e_max
gamma_max = 2 * asin( (1 - R_i/R_e_max) / 2 );

%Mid point for delta = 45Â° (R_e IS NOT KNOWN YET)
%     gamma_mid = 2 * asin( H_tot/2 ./ (2.*R_e.*tan(pi/4)));


%     Cycle on two variables - in this case gamma (inner) and h (
    outer)

%     f_plane = @(x,y,z) a*x+b*y+c==z;
%     f_circle = @(x,y,z) x^2+y^2+c^2==z;

% h = linspace(0,H_tot/2,21);     %Not needed for the current problem
    : if there's a h, the static friction is not needed.

gamma = linspace(gamma_min,gamma_max,63);

R_e = R_i ./ (1 - 2 .* sin(gamma ./ 2));

% [A,Axy] = areeparam(R_i, H_tot, gamma, R_e);
A = zeros(length(gamma),5);
Axy = zeros(length(gamma),2);
delta = zeros(length(gamma),1);

for j=1:length(gamma)

delta(j) = atan((H_tot)/(2*R_e(j)*sin(gamma(j)/2)));

%Areas of projections of all obliquous surfaces on plane xz
A(j,1) = H_tot/2 * (R_e(j) - R_i) / 2;
%Note: there should be a term that includes the curve part but we
%hope it's neglectable.
A(j,2) = H_tot/2 * ((R_i * (1-1/sqrt(2))) + (R_e(j)* (1-cos(pi/8-
    gamma(j)/2)))) /2;
A(j,3) = 2 * ( H_tot/2 * (R_e(j) - R_i) / (2 * sqrt(2)) );
%Note: the area 3 is considered as 2 * area 1 * cos(pi/4).
A(j,4) = H_tot / 2 * (R_e(j) * (sin(pi/8+gamma(j)/2) - sin (pi/8-
    gamma(j)/2)) + R_i /sqrt(2)) / 2;
A(j,5) = 0;

%Area of projections on plane xy (1: triangular, 2: trapezoidal)
Axy(j,1) = R_e(j) * (R_e(j) - R_i) * sin(gamma(j)/2) + R_e(j)^2 * (
    gamma(j)/2 - sin(gamma(j)/2));
Axy(j,2) = (R_e(j) - R_i) * (R_e(j)*sin((pi/4 - gamma(j))/2) + ...
```

```
R_i*sin(pi/8)) + R_e(j)^2 * ((pi/4 - gamma(j))/2 - sin((pi/4 - gamma(
    j))/2)) - R_i^2 * (pi/8 - sin(pi/8));

end

%% Now it's time to cycle!

muvec = [1.05,1.2,1.35];
P_minvec = zeros(size(gamma));

figure(98)
hold on
xlabel('\gamma [rad]');
ylabel('P_{min} [N]');

figure(99)
hold on
xlabel('\delta [deg]');
ylabel('P_{min} [N]');

figure(88)
hold on
xlabel('\Delta \theta [deg]');
ylabel('\Delta x [mm]');

mustring = cell(length(muvec),1);
str = '\mu = ';

for i = 1:length(muvec)
mu = muvec(i);
mustring{i} = sprintf('%s%3.2f',str,mu);

for j=1:length(gamma)

A_param = zeros(5,2);
%A_param has to be initialised every time, otherwise it is possible
%that some elements non-zero in previous iterations remain non-zero
%after, when they would actually be zero.
for k=1:5
A_param(k,1) = A(j,end-(k-1));
A_param(k,2) = A(j,k);
end
Axy_param = Axy(j,:);

Rext_param = R_e(j);
```

```
% Now call the function areae.m with A_param as the input area matrix
    , and Axy_param for the projections on the xy plane
[Atot, Acount] = areae(A_param);

% Now call the function forcex.m and forcey.m that determine the
    amount of force on each direction the static friction is capable
     to hold.
[P_min, P_sol] = forces(Atot, Acount, Axy, F_in, gamma, R_e(j), R_i,
    mu);

P_minvec(j) = P_min;

end

figure(98)
switch i
case 1
plot(gamma,P_minvec,'ko','LineWidth',1.2,'DisplayName',mustring{1});
case 2
plot(gamma,P_minvec,'ks','LineWidth',1.2,'DisplayName',mustring{2});
case 3
plot(gamma,P_minvec,'k^','LineWidth',1.2,'DisplayName',mustring{3});
case 4
plot(gamma,P_minvec,'k*','LineWidth',1.2,'DisplayName',mustring{4});
case 5
plot(gamma,P_minvec,'kv','LineWidth',1.2,'DisplayName',mustring{4});
end


%     delta = atan( H_tot/2 ./ (2.*R_e.*sin(gamma./2)));

dx_vec = 2.*R_e.*sin(gamma);
delta = atan( H_tot/2 ./ (2.*R_e.*sin(gamma./2))) .* (180/pi);

gammadeg = gamma.*(180/pi);
params = [gammadeg', R_e',delta',dx_vec',P_minvec'];

matr = abs(delta.*(pi/180)-pi/3);
index = find(matr == min(matr));

figure(99)
switch i
case 1
plot(delta,P_minvec,'ko','LineWidth',1.2,'DisplayName',mustring{1});
```

```
case 2
plot(delta,P_minvec,'ks','LineWidth',1.2,'DisplayName',mustring{2});
case 3
plot(delta,P_minvec,'k^','LineWidth',1.2,'DisplayName',mustring{3});
case 4
plot(delta,P_minvec,'k*','LineWidth',1.2,'DisplayName',mustring{4});
case 5
plot(delta,P_minvec,'kv','LineWidth',1.2,'DisplayName',mustring{4});
end
figure(99)
hold on
plot(delta(index),P_minvec(index),'ro','LineWidth',1.5,'
    HandleVisibility','off');

end

figure(98)
legend('Location','northwest');
print('gamma','-dpng');
print('gamma','-dsvg');
hold off
figure(99)
legend('Location','northeast');
print('delta','-dpng');
print('delta','-dsvg');
hold off
figure(88)
plot(2.*gammadeg,dx_vec,'ko','LineWidth',1.2,'DisplayName',mustring
    {1});
plot(2.*gammadeg(index),dx_vec(index),'ro','LineWidth',1.5,'
    HandleVisibility','off');
% legend('Location','northeast');
print('dx','-dpng');
print('dx','-dsvg');
hold off

%Now we plot the shapes of the different designs and print the param
    values in a .txt

%[num2str(muvec(i)),'.txt'];        %This is a way to name the file
    using the value of the friction coefficient
name = 'params.txt';
fid = fopen(name,'wt');
fprintf(fid,'gamma\t&\t R_e\t&\t delta\t&\t delta_x\t&\t P_{min}\n');
format long
```

```
for ii = 1:size(params,1)
fprintf(fid,'%3.6g\t&\t',params(ii,:));
fprintf(fid,'\n');
end
fclose(fid);
```

A.2 Function areae.m

```
function [Atot, Acount, ori] = areae(A)
%areae - From the geometrical dimensions of the model and a force
    applied to the piece, it finds the forces that get distributed
    on the surfaces.
%
% Syntax: output = areae([Fx,Fy,Fz], delta, A, Axy)
%
% Long description


% For a quadrant, the surfaces have different reactions to forces
    directed on +x, -x, +y, -y. A quadrant has 5 surfaces, given the
     fact that the axes cut the triangular surfaces in two. We have
    to determine which surfaces react to which forces.
% Because of this we determine a surface orientation, or the normal
    vector to the surface itself. The orientation of the vector is
    the opposite to the force that would encounter resistance by the
     surface, if it was exerted on it.

% For the first quadrant, the components x, y of the normal (they all
     have +1 wrt z):
ori(1,:,:) =   [0, -1; ... %Surf 1
-1, -1; ... %Surf 2
-1,  1; ... %Surf 3
1,  1; ... %Surf 4
1,  0];    %Surf 5

% the other quadrants can be obtained with simple algebric operations
    :
ori(2,:,:) = [1, 0; ... %Surf 1
1, -1; ... %Surf 2
-1, -1; ... %Surf 3
-1, 1; ... %Surf 4
0,  1];    %Surf 5

ori(3,:,:) = [0, 1; ... %Surf 1
1, 1; ... %Surf 2
1, -1; ... %Surf 3
-1, -1; ... %Surf 4
-1, 0];    %Surf 5

ori(4,:,:) = [-1, 0; ... %Surf 1
-1, 1; ... %Surf 2
```

```
1, 1; ... %Surf 3
1, -1; ... %Surf 4
0, -1];    %Surf 5

% Now I create a cell array with matrixes which have the element (j,k
    ) non-zero only if the orientation of the surface is negative in
     (e1,e2), that means they can oppose reaction to forces acting
    on the positive direction of the respective axis. The value in
    the non-zero element is the area of the surface.
% It also computes the sum of the areas of the surfaces that support
    a force in that direction and verse

Atot = zeros(4,1);
Acount = zeros(size(ori));

for qu=1:4
for sur=1:5

if ori(qu,sur,1)<0              %Restraint for case fX>0
Atot(1) = Atot(1) + A(sur,1);
elseif ori(qu,sur,1)>0          %Restraint for case fX<0
Atot(2) = Atot(2) + A(sur,1);
end
Acount(qu,sur,1) = A(sur,1) .* ori(qu,sur,1);

end


end

for qu=1:4
for sur=1:5

if ori(qu,sur,2)<0              %Restraint for case fY>0
Atot(3) = Atot(3) + A(sur,2);
elseif ori(qu,sur,2)>0          %Restraint for case fY<0
Atot(4) = Atot(4) + A(sur,2);
end
Acount(qu,sur,2) = A(sur,2) .* ori(qu,sur,2);

end
end
end
```

A.3 Function forces.m

```
function [P_min,P_sol] = forces(Atot, Acount, Axy, F, delta, R_ext,
    R_in, mu)

%forcex - Description
%
% Syntax: output = forcex(Axtotpos, Atot(2), Axcountpos, Axcountneg,
    P, delta)
%
% Long description

P_sol = zeros(4,5,4);
Forceform = cell(5,2);

% We write here the coefficients for every surface, because obviously
    they are different
% [:,1] +x;     only surfaces 2,3 act
Forceform{2,1} = @(x) ( sqrt( (x*sin(pi/8))^2 + (x*cos(pi/8)*cos(
    delta))) - mu * x * cos(pi/8) * sin(delta) )/ ( sin(delta) + mu
    * cos(delta) );
Forceform{3,1} = @(x) ( sqrt( (x/sqrt(2))^2 + (x*cos(delta)/sqrt(2)))
    - mu * x / sqrt(2) * sin(delta) )/ ( sin(delta) + mu * cos(
    delta) );
% [:,2] -x;     only surfaces 4,5
Forceform{4,1} = @(x) ( sqrt( (x*cos(pi/8))^2 + (x*sin(pi/8)*cos(
    delta))) - mu * x * sin(pi/8) * sin(delta) )/ ( sin(delta) + mu
    * cos(delta) );
Forceform{5,1} = @(x) ( x * cos(delta) - mu * x * sin(delta) )/ ( sin
    (delta) + mu * cos(delta) );
% [:,3] +y;     only surfaces 1,2
Forceform{1,2} = @(x) ( x * cos(delta) - mu * x * sin(delta) )/ ( sin
    (delta) + mu * cos(delta) );
Forceform{2,2} = @(x) ( sqrt( (x*cos(pi/8))^2 + (x*sin(pi/8)*cos(
    delta))) - mu * x * sin(pi/8) * sin(delta) )/ ( sin(delta) + mu
    * cos(delta) );
% [:,4] -y;     only surfaces 3,4
Forceform{3,2} = @(x) ( sqrt( (x/sqrt(2))^2 + (x*cos(delta)/sqrt(2)))
    - mu * x / sqrt(2) * sin(delta) )/ ( sin(delta) + mu * cos(
    delta) );
Forceform{4,2} = @(x) ( sqrt( (x*sin(pi/8))^2 + (x*cos(pi/8)*cos(
    delta))) - mu * x * cos(pi/8) * sin(delta) )/ ( sin(delta) + mu
    * cos(delta) );

F_sur = zeros(4,5,4);
```

```
for qu = 1:4

for sur = 1:5

if F(1)>0 && Acount(qu,sur,1)<0
% We use the Forceform(:,1)

F_sur(qu,sur,1) = - Acount(qu,sur,1)./Atot(1) * F(1);

x =  F_sur(qu,sur,1);
P_res = feval(Forceform{sur,1},x);

if mod(sur,2) == 0
P_sol(qu,sur) = pi*(R_ext.^2 - R_in.^2) ./ Axy(qu,2) .* P_res;
else
P_sol(qu,sur) = pi*(R_ext.^2 - R_in.^2) ./ Axy(qu,1) .* P_res;
end


elseif F(1)<0 && Acount(qu,sur,1)>0
% We use the Forceform(:,1)

F_sur(qu,sur,2) = - Acount(qu,sur,2)./Atot(2) * F(1);

x = F_sur(qu,sur,2);
P_res = feval(Forceform{sur,1},x);

if mod(sur,2) == 0
P_sol(qu,sur) = pi*(R_ext.^2 - R_in.^2) ./ Axy(qu,2) .* P_res;
else
P_sol(qu,sur) = pi*(R_ext.^2 - R_in.^2) ./ Axy(qu,1) .* P_res;
end


end

end

end

for qu = 1:4

for sur = 1:5

if F(2)>0 && Acount(qu,sur,2)<0
```

```
% We use the Forceform(:,2)

F_sur(qu,sur,3) = - Acount(qu,sur,2)./Atot(3) * F(2);

x = F_sur(qu,sur,3);
P_res = feval(Forceform{sur,2},x);

if mod(sur,2) == 0
P_sol(qu,sur) = pi*(R_ext.^2 - R_in.^2) ./ Axy(qu,2) .* P_res;
else
P_sol(qu,sur) = pi*(R_ext.^2 - R_in.^2) ./ Axy(qu,1) .* P_res;
end


elseif F(2)<0 && Acount(qu,sur,2)>0
% We use the Forceform(:,2)


F_sur(qu,sur,4) = - Acount(qu,sur,2)./Atot(4) .* F(2);

x = F_sur(qu,sur,4);
P_res = feval(Forceform{sur,2},x);

if mod(sur,2) == 0
P_sol(qu,sur) = pi*(R_ext.^2 - R_in.^2) ./ Axy(qu,2) .* P_res;
else
P_sol(qu,sur) = pi*(R_ext.^2 - R_in.^2) ./ Axy(qu,1) .* P_res;
end


end

end

end

P_min = max(max(max(P_sol)));

end
```

B MATLAB script results table

$\gamma = \delta\theta$ [deg]	$R_{out}[mm]$	δ [deg]	δx [mm]	P_{min} [N]
6.33425	90.5	71.4787	19.9695	1873.54
6.79281	91.3203	70.0749	21.6026	2158.37
7.25137	92.1554	68.671	23.2642	2464.89
7.70994	93.0058	67.2686	24.9549	2793.51
8.1685	93.8717	65.8694	26.6755	3144.7
8.62706	94.7536	64.4751	28.4265	3518.93
9.08562	95.652	63.0874	30.2089	3916.73
9.54418	96.5673	61.7078	32.0233	4338.66
10.0027	**97.5**	**60.3378**	**33.8706**	**4785.33**
10.4613	98.4506	58.979	35.7516	5257.37
10.9199	99.4195	57.6328	37.6672	5755.46
11.3784	100.407	56.3003	39.6183	6280.34
11.837	101.414	54.983	41.6059	6832.77
12.2956	102.442	53.6818	43.6308	7413.58
12.7541	103.489	52.3979	45.6942	8023.63
13.2127	104.558	51.1322	47.797	8663.86
13.6712	105.649	49.8855	49.9403	9335.25
14.1298	106.762	48.6586	52.1254	10038.8
14.5884	107.898	47.4521	54.3533	10775.7
15.0469	109.059	46.2666	56.6254	11547.1
15.5055	110.243	45.1026	58.9428	12354.2
15.964	111.453	43.9604	61.307	13198.4
16.4226	112.69	42.8403	63.7192	14080.9
16.8812	113.953	41.7425	66.181	15003.4
17.3397	115.244	40.6673	68.6939	15967.4
17.7983	116.564	39.6145	71.2594	16974.5
18.2569	117.913	38.5843	73.8793	18026.5
18.7154	119.294	37.5766	76.5551	19125.4

19.174	120.706	36.5912	79.2887	20272.9
19.6325	122.151	35.6281	82.0821	21471.4
20.0911	123.63	34.687	84.9371	22723
20.5497	125.144	33.7677	87.8558	24030.1
21.0082	126.694	32.8699	90.8403	25395.3
21.4668	128.282	31.9933	93.893	26821.1
21.9254	129.91	31.1375	97.0161	28310.6
22.3839	131.578	30.3023	100.212	29866.7
22.8425	133.287	29.4872	103.484	31492.7
23.301	135.041	28.6918	106.834	33192
23.7596	136.839	27.9158	110.265	34968.4
24.2182	138.685	27.1588	113.78	36825.8
24.6767	140.579	26.4202	117.383	38768.3
25.1353	142.524	25.6998	121.076	40800.5
25.5938	144.522	24.997	124.864	42927.2
26.0524	146.575	24.3115	128.749	45153.5
26.511	148.685	23.6428	132.737	47484.9
26.9695	150.855	22.9905	136.83	49927.4
27.4281	153.086	22.3542	141.034	52487.3
27.8867	155.383	21.7334	145.352	55171.3
28.3452	157.747	21.1278	149.791	57986.8
28.8038	160.181	20.5369	154.354	60941.8
29.2623	162.689	19.9603	159.048	64044.5
29.7209	165.274	19.3977	163.878	67304.3
30.1795	167.94	18.8487	168.851	70730.8
30.638	170.691	18.3128	173.972	74334.9
31.0966	173.529	17.7897	179.249	78128
31.5551	176.46	17.2791	184.69	82122.7
32.0137	179.489	16.7806	190.302	86332.3
32.4723	182.62	16.2938	196.094	90771.7
32.9308	185.858	15.8185	202.074	95456.8

33.3894	189.209	15.3543	208.253	100405
33.848	192.678	14.9008	214.64	105635
34.3065	196.273	14.4578	221.247	111168
34.7651	200	14.025	228.085	117026

Table .1: The results obtained from running the MATLAB script

C CAD model building procedure

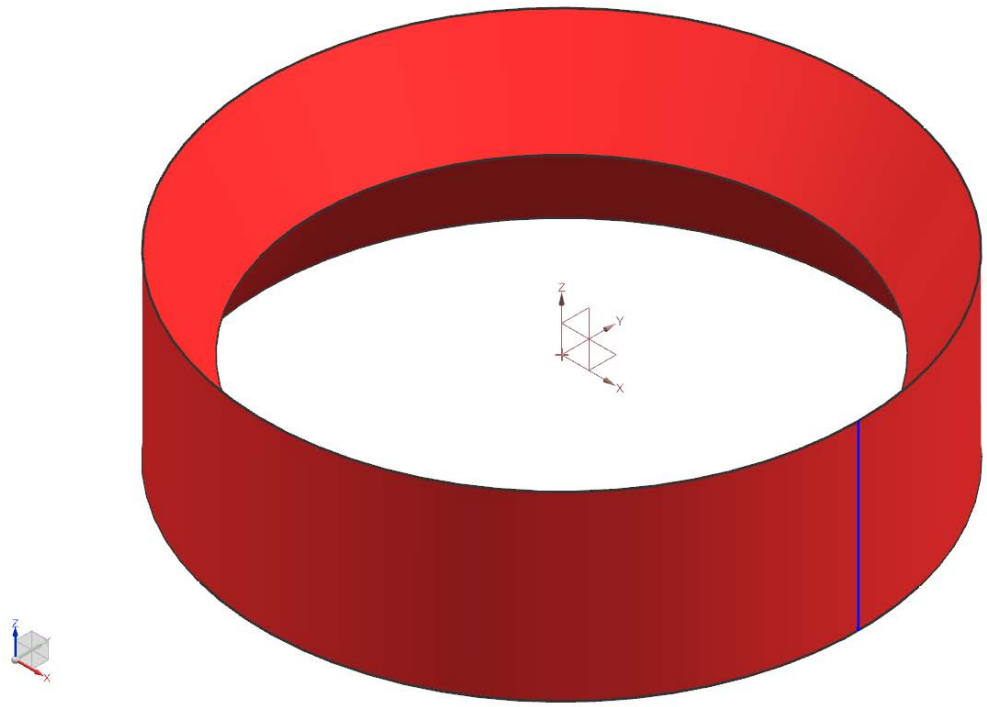

Figure .1: The revolution solid from an isosceles triangle sketched on the xz plane

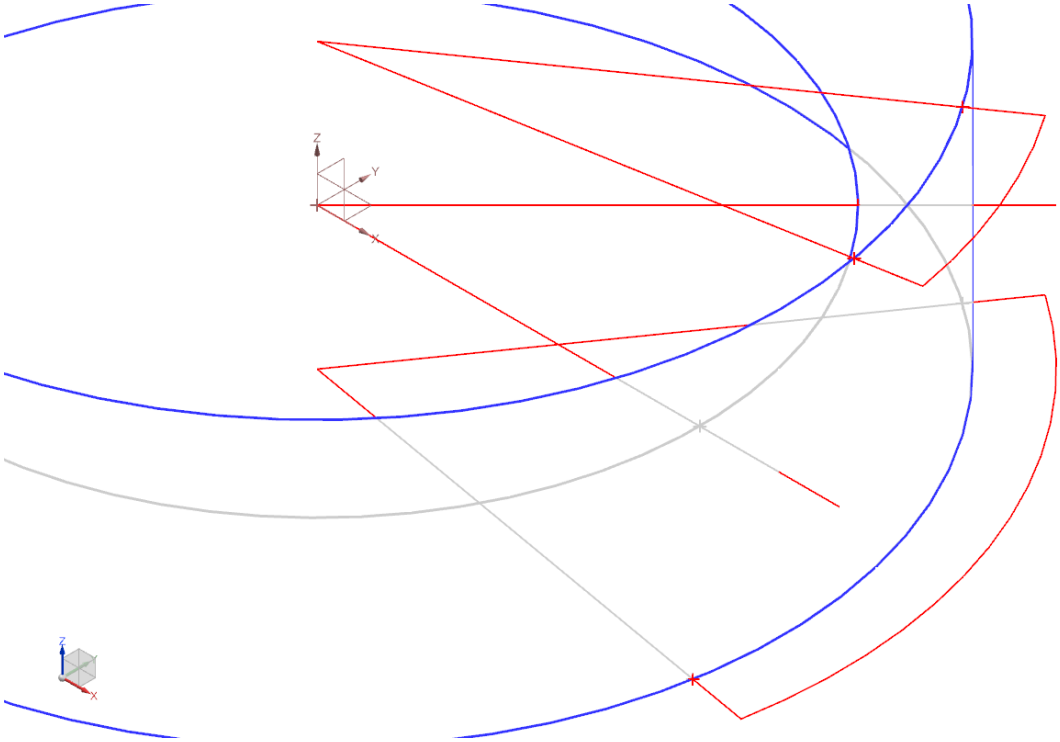

Figure .2: The extremities of the outer edges are traced on one quadrant

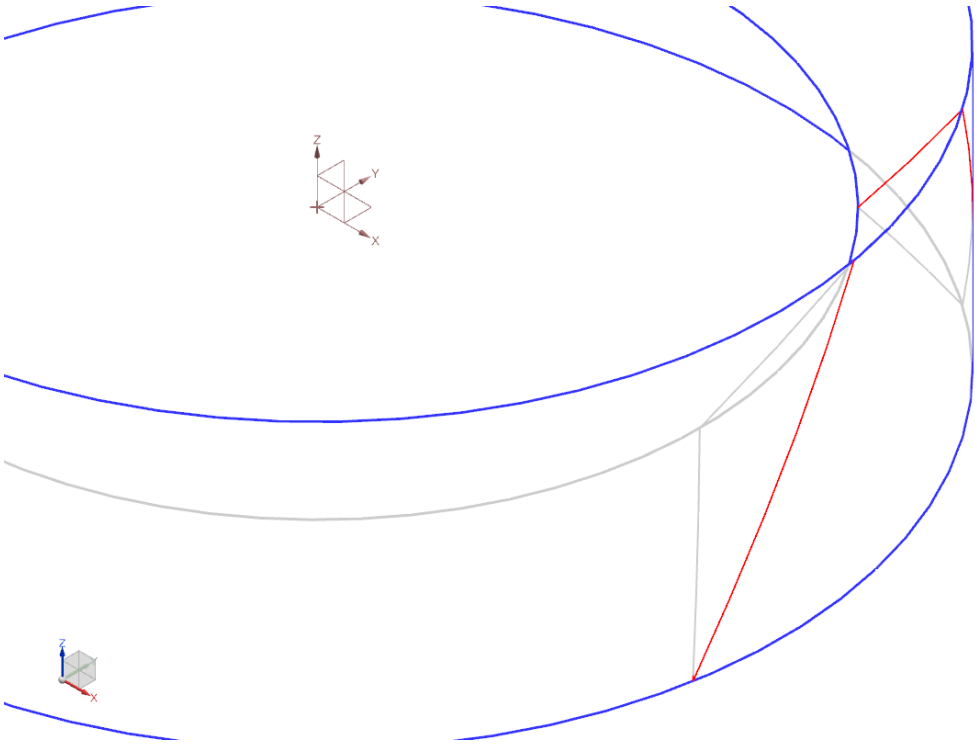

Figure .3: Curves on the faces of the revolution solid are drawn, and surfaces are created using them as sides

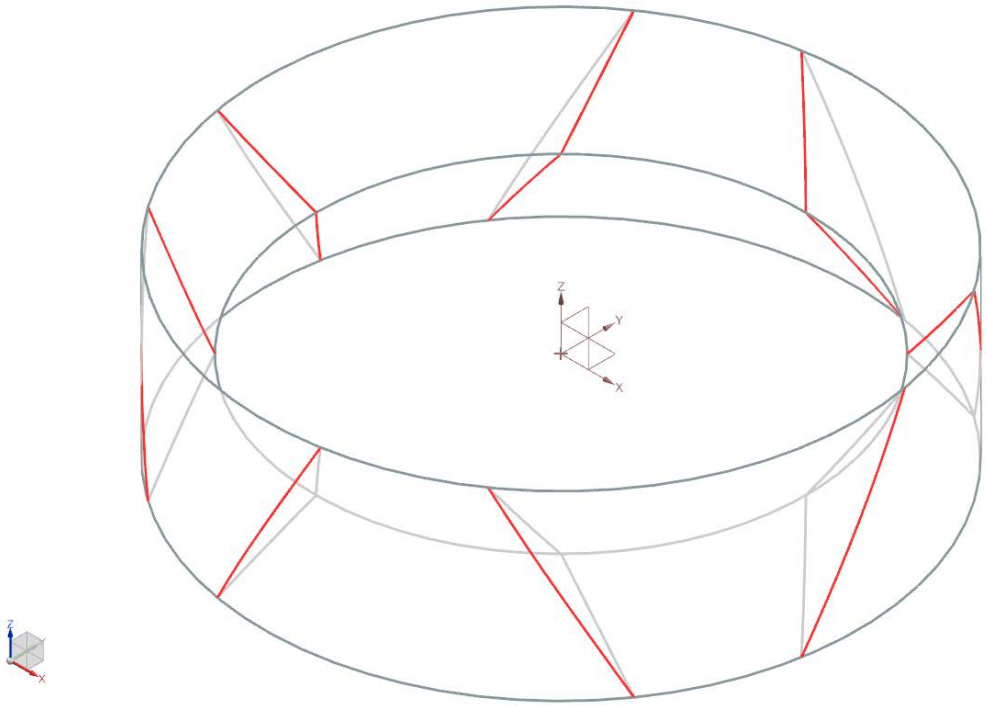

Figure .4: The features created so far on one quadrant are patterned around the circumference

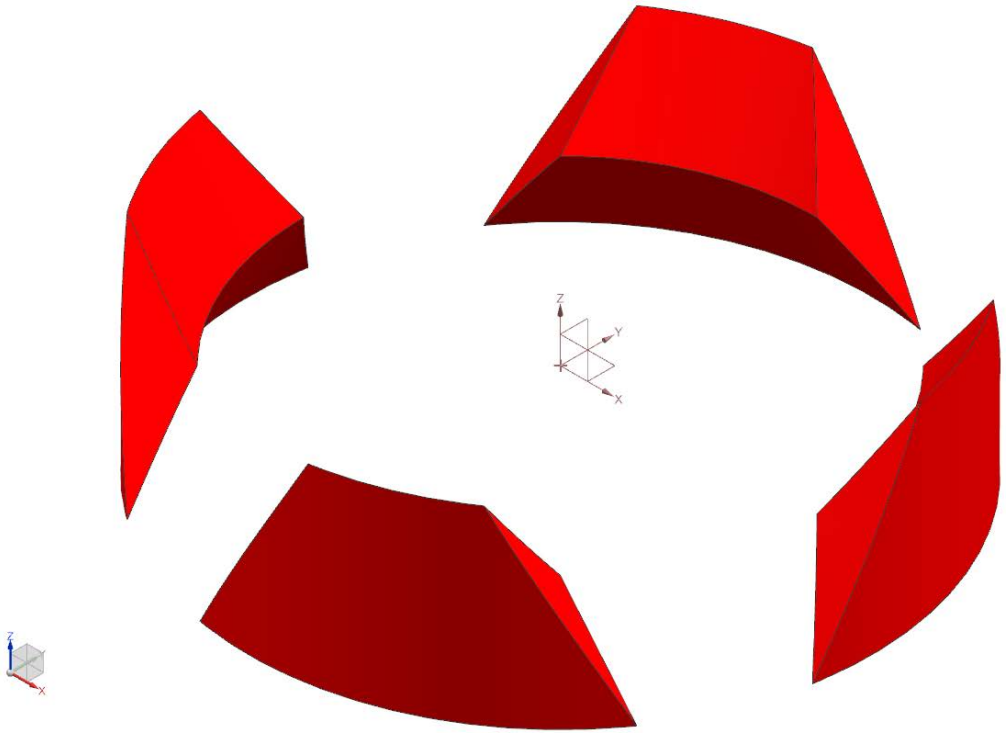

Figure .5: The solid is split and, after importing the geometry to a new model, half of the bodies are suppressed

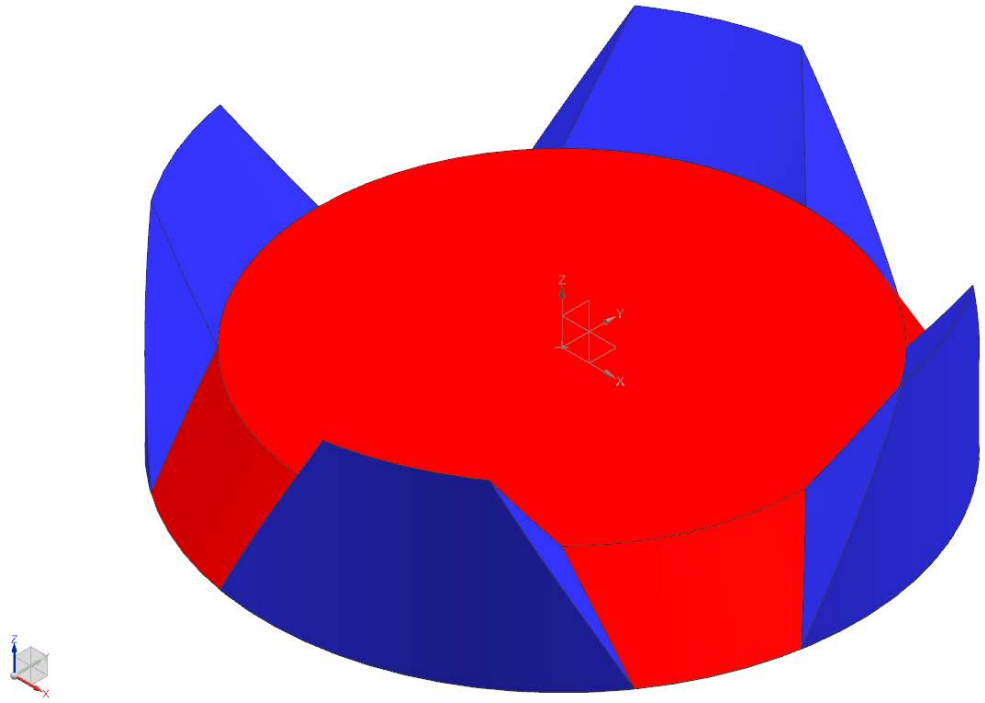

Figure .6: A revolution solid is created: the upper face is the connection plane, the surface obtained from the revolution of the trapezoid's slanted side completes the coupling surface

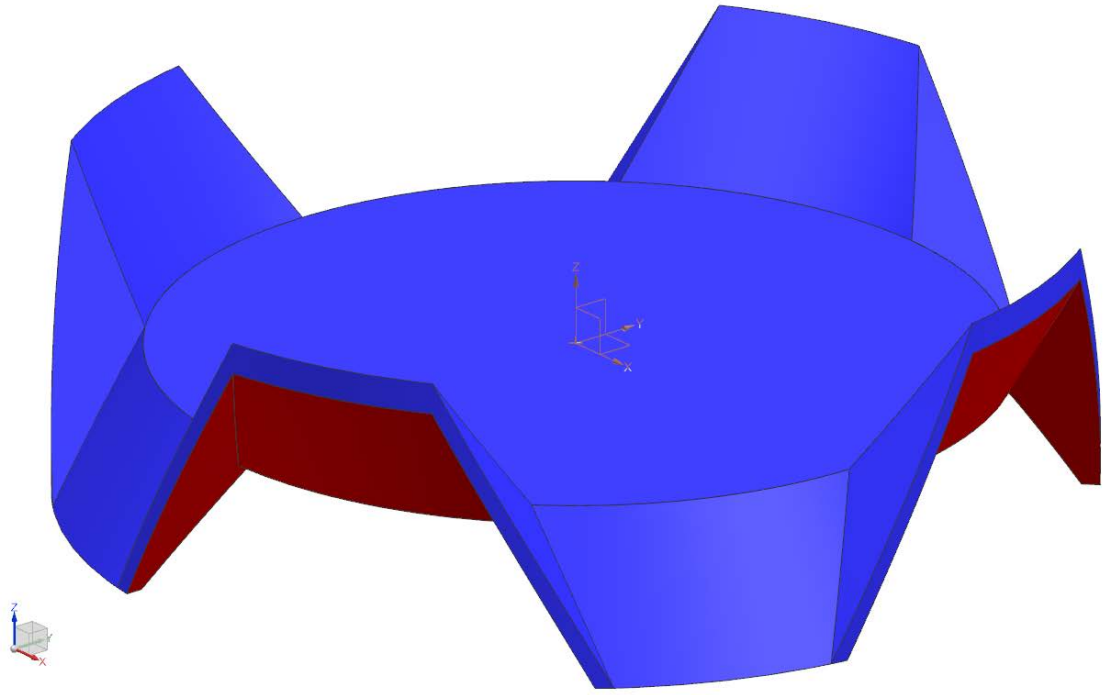

Figure .7: The solid is transformed to a shell, and only the necessary surfaces are kept

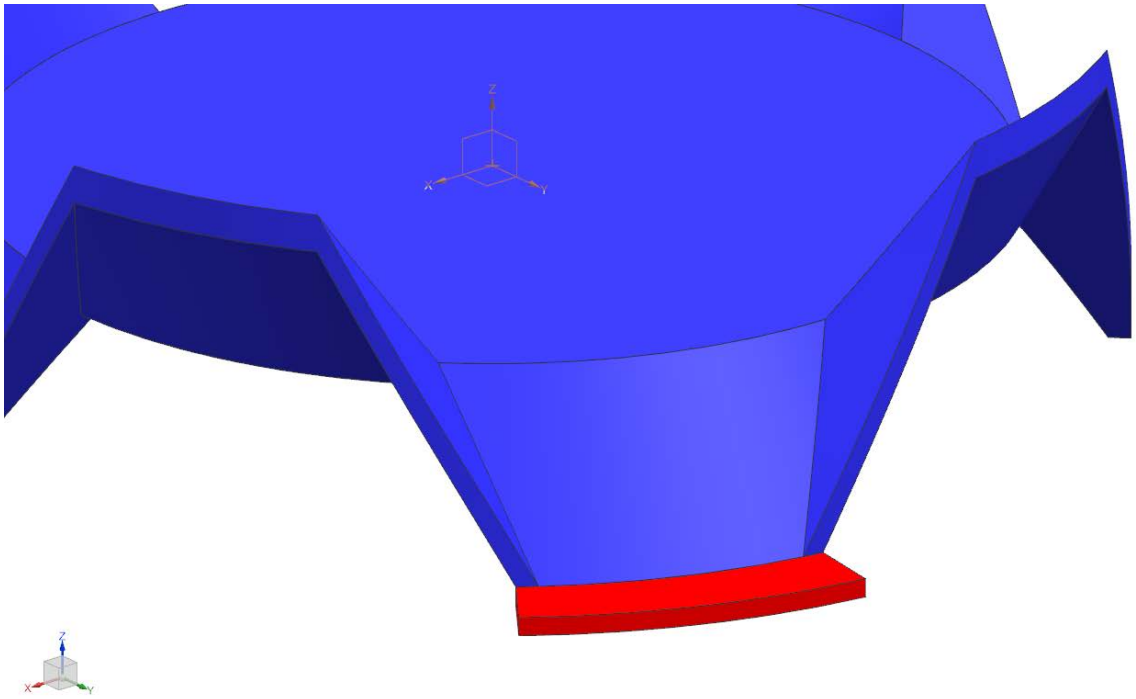

Figure .8: The support flange is created on one quadrant

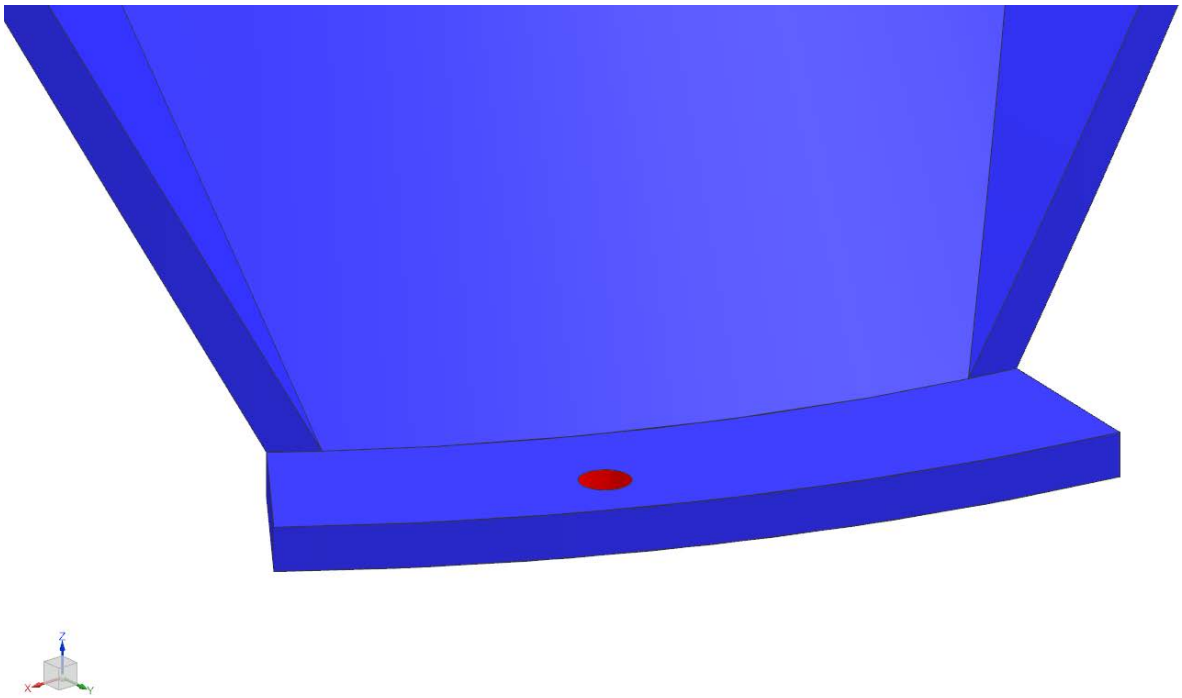

Figure .9: The screw hole is created to match the hole on the base-plate

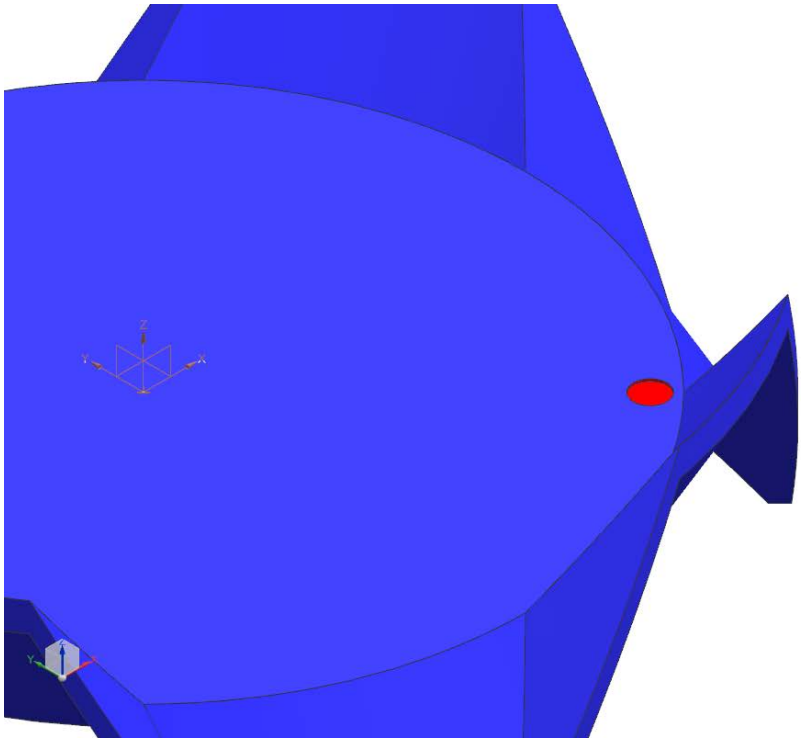

Figure .10: A small recess is created where the screw hole on the meeting plane will be, as an additional safety measure to ensure the screw heads don't protrude from the surface

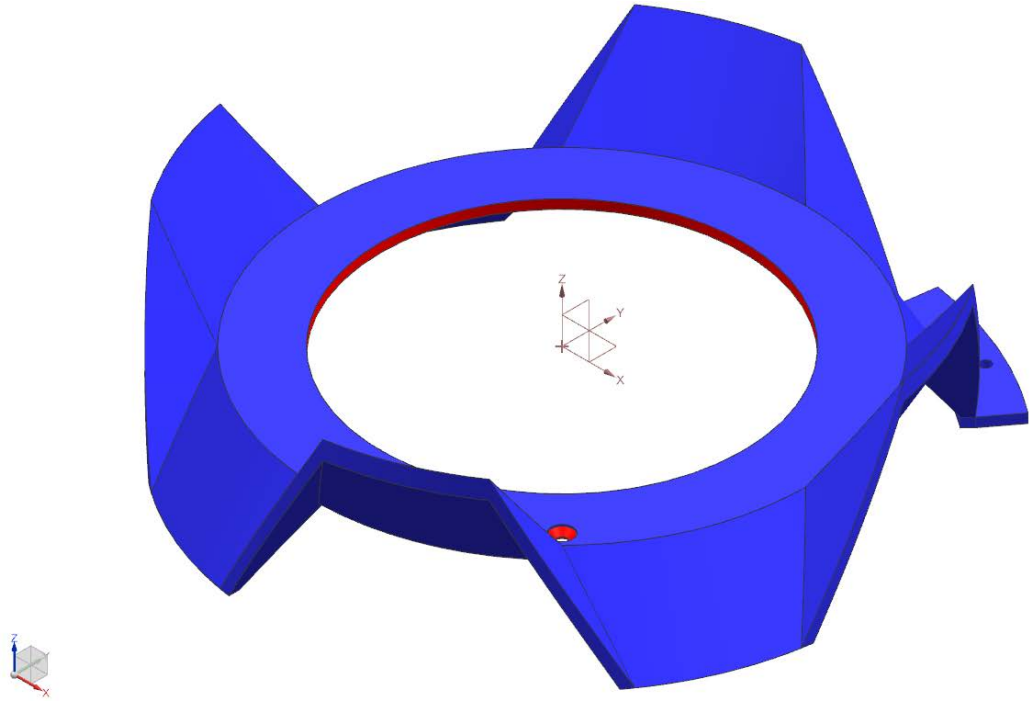

Figure .11: The countersunk screw hole is made in the recess previously created, and the inner surface is hollowed to create a space for the interface to fit in

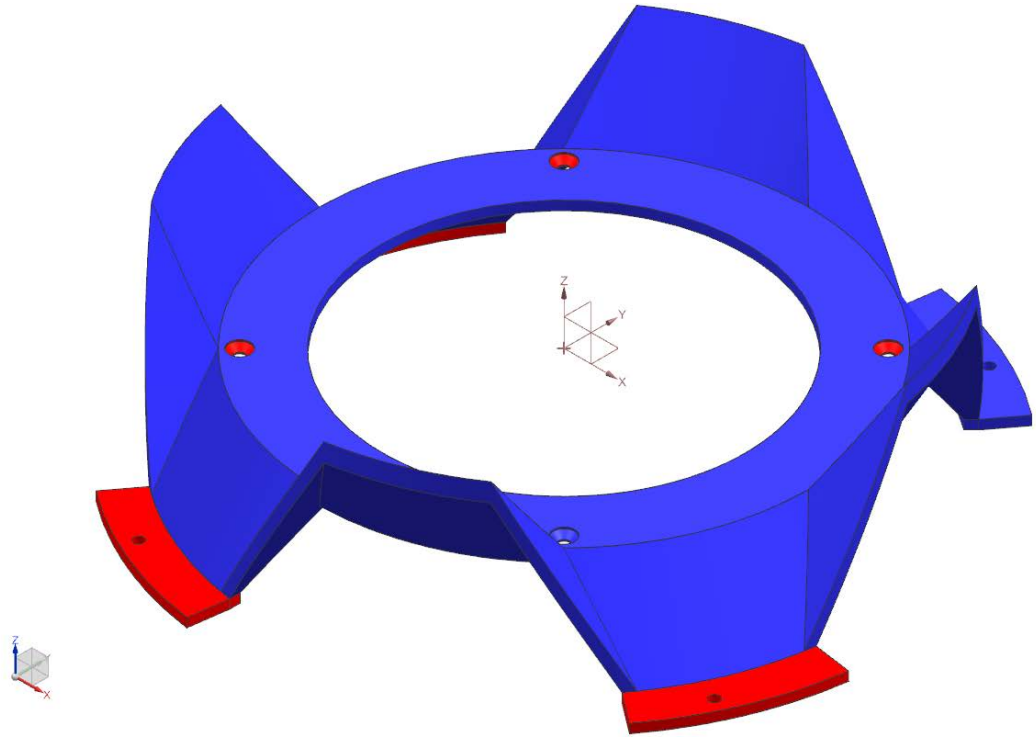

Figure .12: The elements created only in one quadrant are patterned to go around the circumference